PLANT SCIENCES

TAC-C uncovers open chromatin interaction in crops and SPL-mediated photosynthesis regulation

Jingmin Kang[1,2]†, Zhaoheng Zhang[1,3]†, Xuelei Lin[1]†, Fuyan Liu[2]†, Yali Song[2]†, Peng Zhao[1,4], Yujing Lin[1], Xumei Luo[1,3], Xiaoyi Li[5], Yanyan Yang[5], Wenda Wang[5], Cuimin Liu[1], Shengbao Xu[4], Xin Liu[2], Jun Xiao[1,3,6]*

Cis-regulatory elements (CREs) direct precise gene expression for development and environmental response, yet their spatial organization in crops is largely unknown. We introduce transposase-accessible chromosome conformation capture (TAC-C), a method integrating ATAC-seq and Hi-C to capture fine-scale chromatin interactions in four major crops: rice, sorghum, maize, and wheat. TAC-C reveals a strong association between chromatin interaction frequency and gene expression, particularly emphasizing the conserved roles of chromatin interaction hub anchors and hub genes across crop species. Integrating chromatin structure with population genetics data highlights that chromatin loops connect distal regulatory elements to phenotypic variation. In addition, asymmetrical open chromatin interactions among subgenomes, driven by transposon insertions and sequence variations, contribute to biased homoeolog expression. Furthermore, TaSPL7/15 regulate photosynthesis-related genes through chromatin interactions, with enhanced photosynthetic efficiency and starch content in *Taspl7&15* mutant. TAC-C provides insights into the spatial organization of regulatory elements in crops, especially for SPL-mediated photosynthesis regulation in wheat.

INTRODUCTION

Cis-regulatory elements (CREs) are crucial for fine-tuning gene expression, influencing phenotypic diversity, and accelerating crop improvement (*1*–*4*). In rice, a 5.3-kb silencer upstream of the spike development gene *FRIZZY PANICLE* (*FZP*) is bound by Brassinazole 1 (OsBZR1), suppressing *FZP* expression and influencing spike architecture and yield (*5*). In maize, a distal region over 40-kb upstream of *TEOSINTE BRANCHED1* (*TB1*) acts in cis to alter *TB1* transcription, affecting inflorescence structure (*6*). In sorghum, binding by WRKY and ZF-D (zinc finger-DHHC) transcription factors (TFs) activates the aluminum tolerance gene *multidrug and toxic compound extrusion* (*SbMATE*), enhancing tolerance (*7*). These active CREs are typically located in accessible chromatin regions (ACRs) and can act as proximal or distal elements, influencing gene expression locally or over long distances (*8*). Techniques such as assay for transposase accessible chromatin sequencing (ATAC-seq), deoxyribonuclease (DNase)–seq, and formaldehyde-assisted isolation of regulatory elements (FAIRE-seq) have effectively identified ACRs across plant genomes, although they do not capture their spatial organization (*9*–*11*). The number of ACRs correlates with gene density, and in larger genomes, distal ACRs—often functioning as enhancers—are abundant (*12*). These distal elements play a key role in regulating tissue-specific gene expression, particularly in species with large genomes (*13*).

Recent advancements—including chromosome conformation capture (3C) coupled with sequencing (Hi-C), chromatin interaction analysis by paired-end tag sequencing (ChIA-PET), in situ Hi-C followed by chromatin immunoprecipitation (HiChIP), open chromatin enrichment and network Hi-C (OCEAN-C), and chromatin interaction analysis by ATAC (ChIATAC)—have significantly enhanced our understanding of chromatin interactions and three-dimensional (3D) genome structures (*14*–*18*). The dynamics of chromatin loops are crucial for regulating organ development and stress responses in crops (*19*, *20*). The structure of chromatin provides a physical framework for gene regulation by reducing the physical distance between CREs and target genes, and chromatin organization provides a framework for efficient gene regulation, especially in large genome such as maize and wheat, where nuclear metabolic efficiency is vital (*21*, *22*).

Polyploidy, common in crops (*23*), often leads to chromatin structures distinct from those in diploid species, with intersubgenome chromatin interactions forming a novel regulatory layer that supports coordinated gene expression (*24*, *25*). While Hi-C provides a broad view of genome-wide interactions, it may overlook critical contacts between open chromatin and distal regulatory elements (*26*). Techniques such as ChIA-PET and HiChIP offer more specificity, focusing on interactions mediated by DNA binding proteins or histone marks (*14*, *17*). OCEAN-C integrates Hi-C with FAIRE-seq but lacks the signal clarity and TFs binding footprint resolution of ATAC-seq (*27*, *28*). ChIATAC uses SDS treatment of nuclei, producing data distinct from ATAC-seq (*18*). There remains a need for methods that better capture the spatial organization of open chromatin to deepen our understanding of long-range transcriptional regulation.

Common wheat (*Triticum aestivum*) is a widely cultivated allohexaploid crop with a complex genome structure due to its polyploidization, comprising three subgenomes (A, B, and D) and a total genome size of 16G (*29*). This makes wheat an ideal model for exploring the 3D spatial organization of large-genome species. Studies using Hi-C and HiChIP have revealed that interactions within subgenomes are more frequent than those between subgenomes (*30*), indicating a higher-order organization favoring subgenome-specific affinities. ATAC-seq has identified numerous CREs in wheat that play vital roles in gene expression and phenotypic traits (*4*, *31*, *32*). However, the mechanisms by which distal CREs, particularly their

[1]Institute of Genetics and Developmental Biology, Chinese Academy of Sciences, Beijing 100101, China. [2]BGI Research, Beijing 102601, China. [3]University of Chinese Academy of Sciences, Beijing 100049, China. [4]College of Agronomy, Northwest A&F University, Yangling, Shaanxi 712100, China. [5]Institute of Botany, Chinese Academy of Sciences, Beijing 100093, China. [6]Centre of Excellence for Plant and Microbial Science (CEPAMS), JIC-CAS, Beijing 100101, China.
*Corresponding author. Email: jxiao@genetics.ac.cn
†These authors contributed equally to this work.

long-range interactions, regulate gene expression remain poorly understood. High-resolution open chromatin interaction maps generated using OCEAN-C for wheat, and its tetraploid and diploid relatives reveal more frequent chromatin interactions within the D subgenome (*28*), suggesting that it may have evolved more rapidly and retained more epigenetic features from its diploid ancestors. Despite advancements, critical questions remain, such as how specific quantitative trait loci (QTLs) and expression quantitative trait loci (eQTLs) regulate gene expression through long-range interactions, the role of chromatin interactions in homoeolog gene expression bias, and the mechanisms driving chromatin loop formation in wheat.

The establishment and maintenance of nuclear 3D structures have long posed challenges in 3D genome research (*33*, *34*). In animals, the chromatin loop formation is often mediated by CCCTC-binding factor (CTCF) and cohesin complexes (*35*–*37*). The TF Zinc Finger Protein 143 (ZNF143) in animals has been shown to work in tandem with CTCF, regulating CTCF/cohesin interactions and influencing topologically associating domains (TADs) formation (*38*). The lack of a CTCF homolog in plants suggests that any TAD-like structures observed in plants may have evolved through independent pathways (*39*). Recent studies have indicated that in rice (*39*), members of the TCP (teosinte branched1/cycloidea/proliferating cell factor) family of TFs may play a role similar to CTCF in animals. TCPs have been found to recognize specific motifs at the boundaries of rice TAD-like structures (*39*). In addition, TCP TF activity has been linked to 3D chromatin structure regulation in the liverwort *Marchantia* (*40*). Despite these advances, research into TFs mediating 3D genome structures in wheat remains limited. Investigating the roles of specific wheat TFs in nuclear architecture could provide valuable insights into plant genome regulation and evolutionary parallels between plant and animal 3D genome structures.

In this study, we developed the transposase-accessible chromosome conformation capture (TAC-C) technique, integrating in situ Hi-C and ATAC-seq to map fine-scale open chromatin interactions in wheat, rice, maize, and sorghum. We explored the regulatory effects of distal open chromatin on gene expression, focusing on asymmetrical open chromatin interactions within different wheat subgenomes. In addition, we uncovered the key role of SBP (SQUAMOSA promoter binding protein) family TFs in shaping chromatin interactions and their significant impact on regulating photosynthetic energy metabolism in wheat. These findings provide valuable insights and resources for studying 3D genome architecture and transcriptional regulation in complex crop genomes.

RESULTS

TAC-C efficiently capture fine-scale chromatin interactions

To capture chromatin interactions at accessible regions and explore long-range transcriptional regulatory processes in large-genome species with low sequencing depth, we developed a previously unknown strategy. This method integrates ATAC-seq with Hi-C, resulting in a more efficient technique we term TAC-C. Plant tissue was first fixed with formaldehyde, followed by the extraction of high-quality nuclei. To better preserve open chromatin regions, we avoid SDS treatment and instead perform in situ restriction enzyme digestion directly using with Dpn II, followed by biotin labeling and proximity ligation, slightly differing from traditional in situ Hi-C protocol. Next, we apply transposase for in situ tagmentation, following the ATAC-seq protocol. Biotin-labeled chromatin ligation products are isolated using biotin-streptavidin affinity, and the TAC-C library is generated through polymerase chain reaction (PCR) (Fig. 1A and see Methods for details).

The TAC-C data exhibited high reproducibility between biological replicates (fig. S1A and table S1). At the chromosome level, TAC-C interaction maps exhibited robust signals along primary diagonals and anti-diagonal lines (Fig. 1B and fig. S1B), reflecting a Rabl-like chromosome configuration consistent with Hi-C data (*30*). This indicates that TAC-C effectively captures the high-order organization of the wheat genome. To assess TAC-C's ability to capture accessible chromatin regions, we compared it with ATAC-seq libraries from leaf tissues at the same developmental stage (Fig. 1C). As sequencing depth increased, the number of peaks identified by TAC-C, OCEAN-C (*28*), and ATAC-seq (datasets generated by (*28*) and this study) also increased. However, TAC-C and OCEAN-C consistently identified fewer peaks than ATAC-seq, as they specifically capture open chromatin regions involved in interactions. Notably, at the same sequencing depth, TAC-C detected many more peaks than OCEAN-C, reaching saturation at 80-Gb sequencing depth. The 78.5% of TAC-C peak-covered regions overlapped with ATAC-seq, indicating high similarity, whereas only 46.6% of OCEAN-C peak-covered regions overlapped with its corresponding ATAC-seq library (fig. S1C). To determine whether Dpn II affects open chromatin capture, we replaced it with bovine serum albumin (BSA) while keeping other conditions unchanged. The BSA-based library showed peak-covered regions highly similar to ATAC-seq and TAC-C (fig. S1D), confirming that TAC-C library preparation has minimal impact on open chromatin capture.

In wheat, we identified 332,927 overlapping TAC-C peaks from two biological replicates (Rep1: 398 M read pairs; Rep2: 405 M read pairs) for subsequent analysis. These peaks were categorized into gene body (g, 36.7%), promoter (p, 33.7%), and distal (d, 29.6%) CREs (Fig. 1D). Comparing peak distributions, TAC-C and ATAC-seq signals were strongly enriched at transcription start sites (TSSs), largely more than OCEAN-C (Fig. 1E). Correlation with epigenetic marks revealed that TAC-C peaks were predominantly associated with active histone modifications (H3K4me3, H3K9ac, and H3K27ac), similar to OCEAN-C but much higher than ATAC-seq and Hi-C (*25*, *41*) (Fig. 1F). This indicates TAC-C peaks are mainly located in active CREs, such as promoters or enhancers. In addition, the genomic distribution of TAC-C specific peaks (not overlapping with ATAC-seq; Fig. 1C), closely resembled that of shared TAC-C and ATAC-seq peaks (fig. S1E). Although histone modification enrichment was slightly lower in these unique TAC-C peaks, it remained comparable to ATAC-seq (fig. S1F), suggesting that they may represent genuine regulatory regions not captured by ATAC-seq rather than artifacts of TAC-C library preparation.

We further compared TAC-C with OCEAN-C and Hi-C in identifying chromatin interactions. Consistent with previous study (*25*), we observed more frequent interactions between chromosomes within the same subgenome in TAC-C (fig. S1G). TAC-C identified 159,667 intrachromosomal loops (table S2), which were classified into proximal anchors (P) located within 3 kb of a gene's TSS and distal anchors (D) beyond 3 kb. These loops comprised 55.5% P-P interactions (PPIs), 35.5% P-D interactions (PDIs), and 9.0% D-D interactions (DDIs) (Fig. 1G). Compared to OCEAN-C and Hi-C, TAC-C detected a higher proportion of PPIs and identified shorter

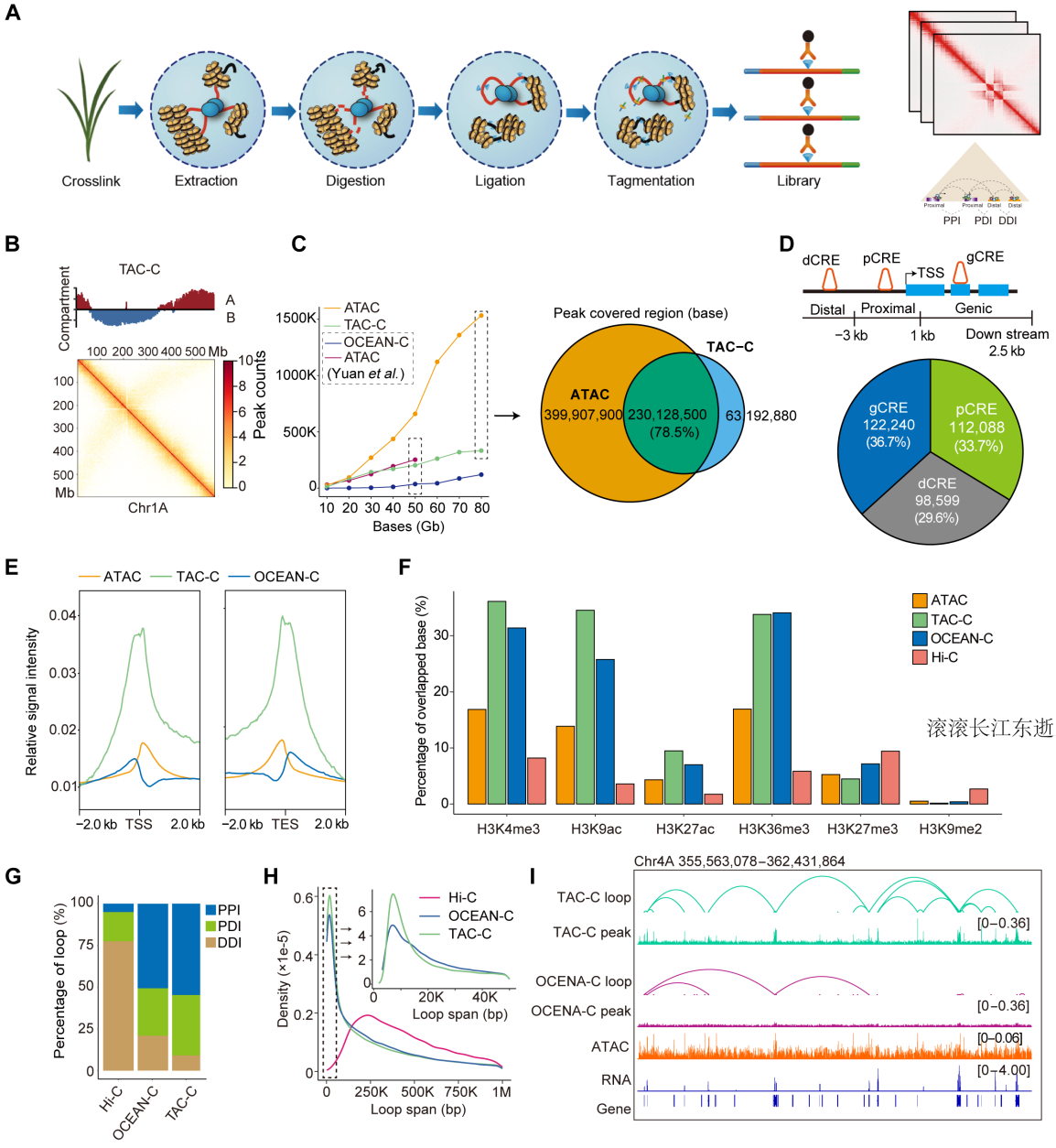

Fig. 1. Identification of open chromatin interactions using TAC-C and comparison with other techniques. (**A**) Schematic of TAC-C. (**B**) TAC-C interaction matrix at 1-Mb resolution across chromosome 1A, with chromatin compartments shown as a track above the contact map. Compartment A is marked in red, and compartment B is marked in blue. (**C**) Statistical comparison of peak capture efficiency under different sequencing depth using TAC-C, ATAC, and OCEAN-C. Venn diagram showing the overlap of peak-covered region between ATAC and TAC-C based on 80 Gb of sequencing depth. (**D**) Classification of CREs based on their distribution around genes, with the number and proportion of each CRE type of CRE indicated. TSS, transcription start site; dCRE, distal CRE; pCRE, proximal CRE; gCRE, genic CRE. (**E**) Relative signal intensity of TAC-C, OCEAN-C, and ATAC around TSS and transcription termination site (TTS). (**F**) Percentage of overlapped base of TAC-C, OCEAN-C, Hi-C, and ATAC peaks with various histone modification marks. (**G**) Percentage of proximal-proximal interactions (PPIs), proximal-distal interactions (PDIs), and distal-distal interactions (DDIs) identified by TAC-C, OCEAN-C, and Hi-C. (**H**) Loop span distribution of open chromatin interactions identified by TAC-C, OCEAN-C, and Hi-C. Regions with loop span below 50 kb are highlighted in the top right corner. (**I**) Example of open chromatin interactions: Browser view of a 7-Mb region showing a randomly selected open chromatin interactions with associated TAC-C and OCEAN-C data.

loop spans (Fig. 1H), indicating its superior performance in capturing fine-scale open chromatin interactions (Fig. 1I).

In summary, we have developed the TAC-C assay by integrating in situ Hi-C and ATAC-seq protocols, validating it experimentally in bread wheat. This method enhances the ability to capture open chromatin interactions, particularly in large-genome crops such as wheat.

Conserved features of chromatin interactions across four crop species

To evaluate the broad applicability of TAC-C across species and investigate open chromatin interactions in crops, we performed TAC-C experiments on young leaves from rice (*Oryza Sativa*), sorghum (*Sorghum Bicolor*), and maize (*Zea Mays*). We observed

high reproducibility between biological replicates (Pearson's correlation of 0.91 to 0.99) and consistent chromosome configurations as reported (*20*, *42*, *43*), as well as expected genomic distribution pattern of peaks (figs. S1A and S2, A and B). The number of identified loops ranged from 46,327 to 159,667 across species, with larger genomes exhibiting more loops (Fig. 2A and fig. S3A). Notably, *Z. mays* and *T. aestivum* with large genome sizes displayed longer open chromatin interactions and a higher proportion of PDI and DDI compared to smaller genomes (*O. sativa* and *S. bicolor*) (Fig. 2B and fig. S3, B and C).

PPIs serve as key spatial units of gene regulation (*42*). To examine the relationship between looped genes, we categorized genes in a looped pair ("Gene a") into three groups (0 to 20%, 20 to 80% and 80 to 100% percentile) according to the expression level of one and compared the expression levels of its paired gene ("Gene b") (fig. S3D). The results showed that as "Gene a" expression increased, "Gene b" expression also rose, while the expression levels of random gene pairs remained consistently low. This suggests that chromatin interactions establish physical connections between distant genes, enabling coordinated regulation. To further assess the relationship between interaction frequency and gene expression, we ranked genes into four interaction levels (L1: 0 to 25%; L2: 25 to 50%; L3: 50 to 75%; L4: 75 to 100%). Across all four species, genes with higher interaction frequencies exhibited increased expression (Fig. 2C and fig. S3E), underscoring the regulatory significance of highly interacting genes.

The top 10% most frequently interacting anchors were defined as "hub anchors," while other anchors were designated as "connecting anchors." Open chromatin peaks not located in loop anchors were categorized as "basal peaks." Genes linked to hub anchors were termed as "node genes," whereas those associated with connecting anchor were "connecting genes" (Fig. 2D and fig. S3F) (*44*). Hub anchors exhibited higher TAC-C signals (Fig. 2E) but no change in chromatin accessibility (fig. S3G), indicating that TAC-C signals reflect interaction strength rather than accessibility (fig. S3H). Node genes exhibited lower single-nucleotide polymorphism (SNP) densities, higher expression levels across four species (Fig. 2, F and G) (*45*–*48*), and the highest proportion of orthologs across species, followed by connecting genes (Fig. 2H). Thus, genes involved in frequent looping events may have more important functions.

Overall, open chromatin interaction span and frequency are influenced by genome size and gene counts across species. These

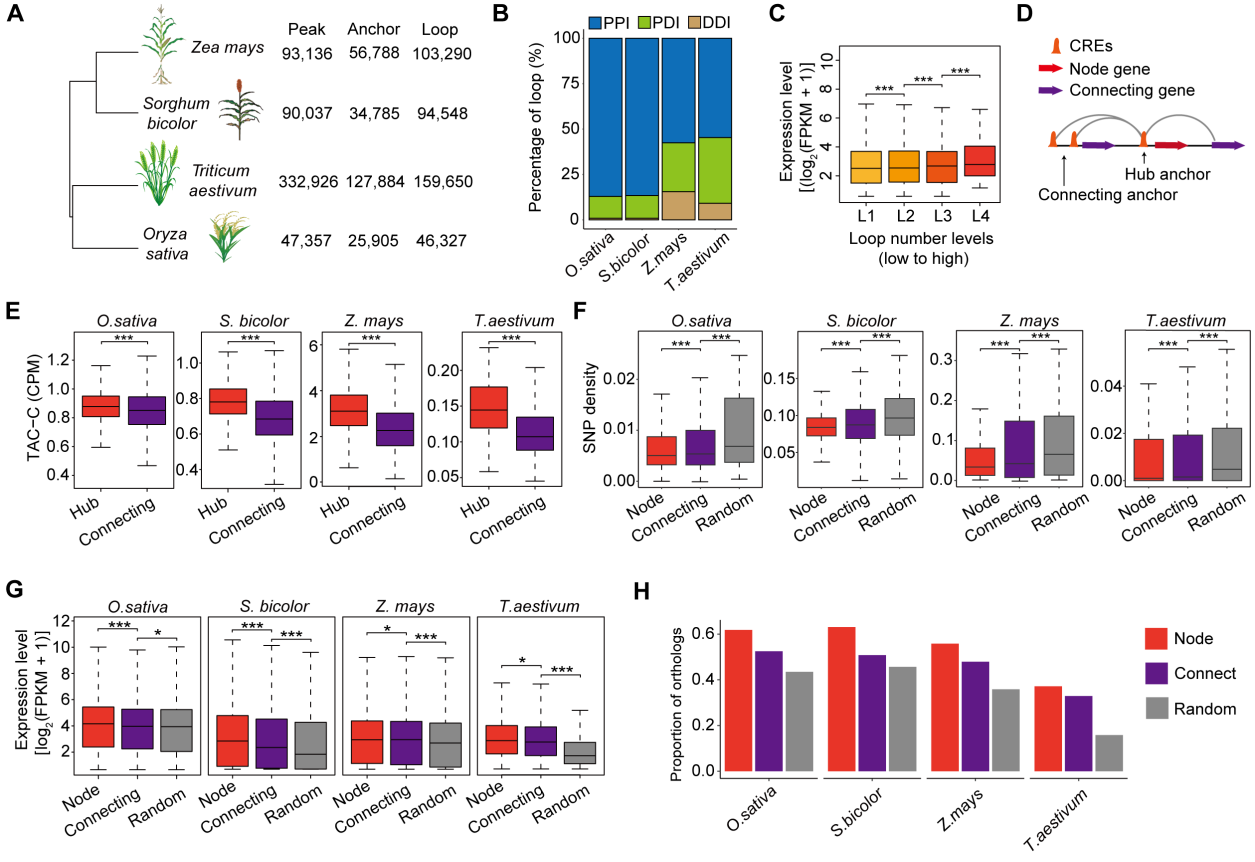

Fig. 2. Characteristics of chromatin interactions across four crops species. (**A**) Phylogenetic tree of four crop species with the number of peaks, anchors, and loops identified from TAC-C data. (**B**) Percentage distribution of PPI, PDI, and DDI across the four crop species. (**C**) Expression levels [$\log_2$(FPKM + 1)] of genes with varying levels of chromatin interactions in *T. aestivum*. ***$P < 0.001$ from Student's *t* test. (**D**) Schematic representation of the hub-and-connection anchor model of chromatin interactions, with definitions of for node and connecting genes based on contact frequency. (**E**) TAC-C signal intensity in hub and connecting anchor regions across the four crop species. ***$P < 0.001$ from Student's *t* test. (**F** and **G**) SNP density (F) and expression levels (G) in node, connecting, and random genes across the four crop species. *$P < 0.05$, and ***$P < 0.001$ from Student's *t* test. (**H**) Percentage of orthologs in node, connect, and random genes across four crop species. The ortholog information from TGT (http://wheat.cau.edu.cn/TGT/).

interactions facilitate coordinated gene expression and are regulated by chromatin interaction frequency. Hub anchors and hub genes are highly conserved, highlighting their fundamental biological roles.

Chromatin interaction link regulatory elements to phenotype variation in wheat

To explore the importance of spatial organization of chromatin, we compiled data from published sources on QTLs and eQTLs related to various agronomic traits (table S3), as well as breeding selection sweeps (SSs) in wheat to investigate whether chromatin interactions could spatially link distal regulatory elements to target genes, ultimately contributing to phenotypic variation (*49*–*52*). Our analysis revealed that hub anchors, which primarily localize to the distal ends of chromosomes, showed a distribution pattern consistent with "functional regions" as defined by QTLs, eQTLs, and SS (Fig. 3A). Notably, hub anchors exhibited the highest overlap with these functional regions, followed by connecting anchors and basal peaks (Fig. 3B), suggesting that regions frequently involved in chromatin loops may play more crucial roles in gene regulation. Furthermore, QTLs overlapping with hub anchors exhibit stronger significance, while eQTLs and genes looped by hub anchors demonstrate larger effect sizes (*50*, *53*) (Fig. 3, C and D). In addition, QTL regions associated with loops are enriched in activating histone modifications (H3K4me3 and H3K27ac) as well as H3K27me3, whereas H3K9me2 is not enriched (fig. S4). This suggests that these regions may function as active or bivalent enhancer elements (*54*).

In total, 7632 hub anchors overlapped QTLs, eQTLs, and breeding selection sweeps. Of these, only 259 hub anchors were common across all three regions (Fig. 3E). For instance, an eQTL (Chr5A_645725) located 621 kb downstream of the leaf width-regulated gene *NARROW LEAF1* (*TaNAL1-like-5A*) was found within a flag leaf area (FLA)–regulated QTL and a breeding selection region (*50*, *55*, *56*). This eQTL, located in a hub anchor, was observed to loop with *TaNAL1-like-5A* (Fig. 3F). Furthermore, the functional potential of these distal regulatory regions was established through a luciferase reporter assay. *TaNAL1-like-5A* carrying the distal regions exhibited robust activity in the reporter assay, with higher signals compared with the controls carrying the 35*S* promoter alone (Fig. 3G). These findings suggest that distal regulatory elements can modulate target gene expression through chromatin interactions, thereby influencing phenotypic variation. To explore the genetic variation underlying this regulation, haplotype analysis was conducted for both *TaNAL1-like-5A* and the distal eQTL region Chr5A_645725 (Fig. 3F) (*57*). This analysis identified three distinct haplotypes, each exhibiting significant differences in flag leaf length, width and flag leaf area across various natural populations (Fig. 3H) (*57*).

Our findings reveal that distal elements may regulate the expression of target genes through chromatin interactions, thereby influencing phenotypic variation. Providing physical topological information support for distal regulatory sites identified through genome-wide association studies (GWAS) and transcriptome-wide association studies (TWAS).

Asymmetric chromatin interaction associates with homoeolog expression bias in wheat

Because wheat is a hexaploid species, with proportion of A, B, and D subgenomes showing imbalanced expression patterns (*58*), we wondered whether differences in chromatin interactions among subgenomes contribute to this expression bias. We compared the loops at subgenomic levels for each chromosome. While the strength of the loops was comparable across three subgenomes, the D subgenome exhibited significantly more loops than the A and B subgenomes, consistent with previous study (fig. S5, A and B) (*28*). In total, 39,714, 36,643, and 41,559 PPIs were identified in A, B, and D subgenomes, respectively. Among these, 3,742, 5,337 and 5,257 PPIs were conserved between two AB, AD, and BD subgenomes, respectively. Also, 7504 PPIs were conserved across all three subgenomes (Fig. 4A), indicating asymmetrical interactions between subgenomes.

The coverage of transposable elements (TEs) in singleton loops was significantly higher than that in homoeolog PPIs across subgenomes, suggesting a link between transposon insertion and the occurrence of asymmetrical interactions (Fig. 4B). The loop strength for ABD-conserved PPIs was the highest, while singleton PPIs exhibited the weakest loop strength (Fig. 4C). In addition, 56.7% of loop anchors for ABD-conserved PPIs were classified as hub anchors, indicating that ABD-homoeolog interactions may represent crucial regulatory regions (Fig. 4D). Furthermore, homoeolog PPIs demonstrated a higher overlap with functional regions (Fig. 4E), and Gene Ontology (GO) enrichment analysis revealed that genes associated with conserved PPIs are primarily involved in carbohydrate metabolism, photosynthesis, and growth and development (fig. S5C). In contrast, genes located in singleton loops were mainly enriched in basic cellular processes (fig. S5D).

To evaluate the impact of asymmetrical PPIs on homoeolog expression bias, we analyzed 16,539 triads with at least one homoeolog linked to a loop. As expected, expression levels remained unchanged in ABD-conserved PPI-linked homoeologs. However, in PPIs conserved in only two subgenomes (AB, AD, and BD), the homoeolog lacking loops showed significantly lower expression than the other two (Fig. 4F). In addition, ABD-conserved PPI-linked genes had the highest proportion of balanced expression triads, while homoeologs missing loops were more likely to be suppressed in AB-, AD-, or BD-conserved PPIs (Fig. 4G). Similar trends were observed in chromatin accessibility differences of triads with asymmetric PPIs among subgenomes (fig. S5E). Further analysis of homoeolog pairs with differential interactions but balanced chromatin accessibility confirmed that, except for the AD group, asymmetrical interactions and chromatin accessibility bias both contribute to homoeolog expression bias (fig. S5F).

To explore the relationship between epigenetic modifications and asymmetrical PPIs, we analyzed histone modifications in the 5-kb regions flanking asymmetrical loop-linked homoeolog triads. Activation histone marks, specifically H3K36me3 and H3K9ac, correlated with PPI asymmetry levels, with homoeologs lacking loops exhibiting lower coverage of these histone marks (Fig. 4H). In contrast, other epigenetic signals (H3K27ac, H3K4me3, and H3K27me3) showed no significant differences (fig. S5G). For instance, a homoeolog triad (*TraesCS1A03G0004300*, *TraesCS1B03G0002100*, and *TraesCS1D03G0000500*) formed loops with another triad (*TraesCS1A03G0005200*, *TraesCS1B03G0003300*, and *TraesCS1D03G0001500*) in the B and D subgenomes, but not in the A subgenome (Fig. 4I). These asymmetrical loops were associated with elevated expression levels and enriched activating chromatin modifications in the B and D homoeologs. A similar pattern was observed in another case where a homoeolog pair lost loops in the B subgenome (fig. S5H).

To further understand the factors driving asymmetrical PPIs, we compared TE coverage and sequence similarity in the 5-kb regions flanking the asymmetrical loop-linked homologous triads (Fig. 4, J

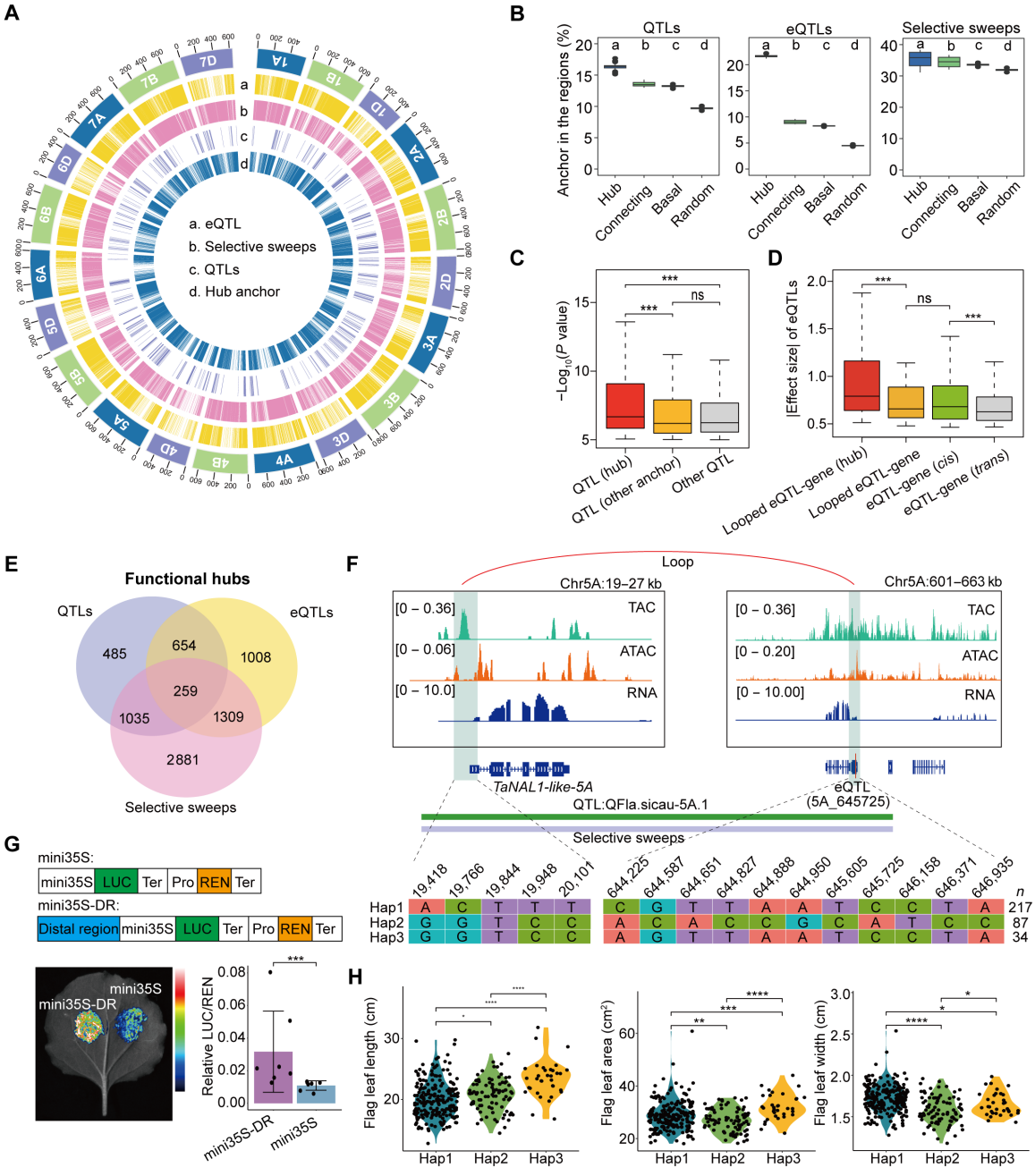

Fig. 3. Long-range chromatin interactions regulate gene expression and associate with trait variations. (**A**) Distribution of wheat eQTLs (a), breeding selective sweeps (b), QTLs (c), and hub anchors (d) across the wheat genome. (**B**) Percentage of overlapping interactions between hub anchors, connecting basal anchors, and random regions with QTLs, eQTLs, and breeding selective sweeps. To reduce false positives, 1000 permutation tests were conducted. In each test, 60% of accessions were randomly sampled, and differences were calculated using least significant difference (LSD) test. (**C**) Significance of GWAS signals for SNPs located in hub anchors, other anchors, and QTL regions. GWAS signal data were obtained from published sources (details in table S3). ***$P < 0.001$ and ns (not significant), $P > 0.05$ from Student's *t* test. (**D**) |Effect size| of looped eQTL-gene pairs compared to other eQTL-gene pairs. Looped eQTL-gene (hub) pairs refer to those where the eQTL is located in anchors or hub anchors. Effect size data were obtained from published studies, and only eQTLs in the top 50% of effect size were included (details in table S3). ***$P < 0.001$ and ns, $P > 0.05$ from Student's *t* test. (**E**) Overlap between hub anchors, QTLs, eQTLs, and breeding selective sweeps. (**F**) Open chromatin loop between *TaNAL1-like-5A* and distal eQTL (5A_645725). Green and pink tracks indicate QTL and breeding selection sweep regions. The table below shows haplotypes of SNP sites in *TaNAL1-like-5A* and the distal regulatory region. (**G**) Luciferase reporter assays validating the transcriptional regulatory role of the distal region on *TaNAL1-like-5A*. The distal anchor sequences, containing the eQTL locus, were introduced into the proximal region of *TaNAL1-like-5A* promoter (distal region). ***$P < 0.001$ from Student's *t* test. (**H**) Flag leaf length, width, and leaf area of *TaNAL1-like-5A* in three haplotypes of the loop- linked *TaNAL1-like-5A* and eQTL (5A_645725). *$P < 0.05$, **$P < 0.01$, ***$P < 0.001$, and ****$P < 0.0001$ from Student's *t* test.

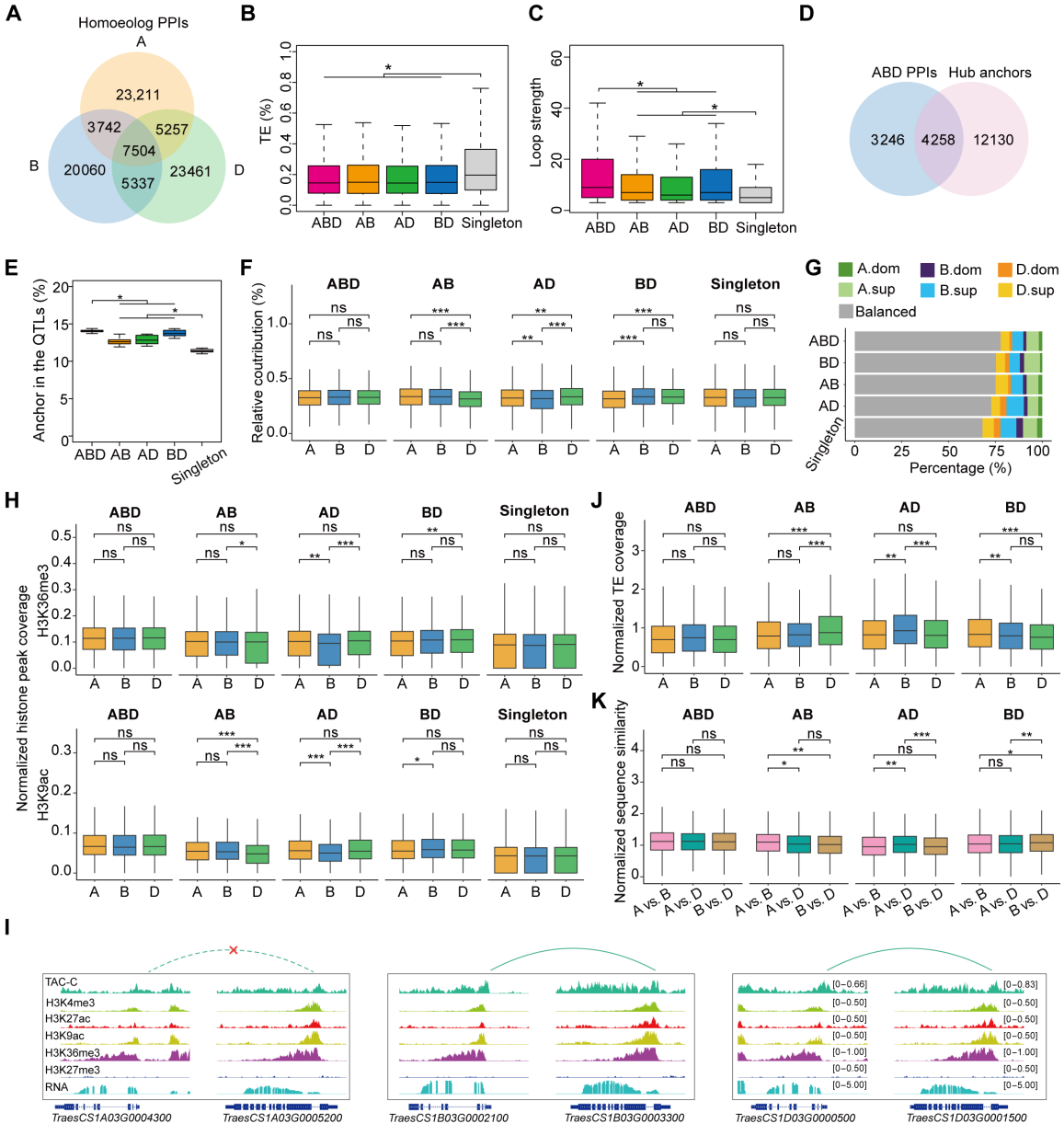

Fig. 4. Asymmetrical open chromatin loops associated with homoeolog expression bias, epigenetic profiling, TE insertions, and sequence variations. (**A**) Venn diagram showing the overlap of homoeolog PPIs between the A, B, and D subgenomes. (**B** and **C**) Boxplots illustrating the TE coverage (B) and loop strength (C) across loop anchors at different homoeolog levels. ABD: homoeolog PPIs in all three subgenomes; AB, AD or BD: homoeolog PPIs in AB, AD or BD subgenomes; singleton: PPIs in only one of the subgenomes A, B or D. *$P < 0.05$ from Student's *t* test. (**D**) Venn diagram showing the overlap between homoeolog ABD PPIs and hub anchors. (**E**) Overlap ratio of QTL regions with PPI anchors at different homoeolog levels, normalized by the average QTL coverage in A, B, and D subgenomes, respectively. (**F**) Relative expression contribution of each subgenome based on triads, classified into five groups according to homoeolog PPI levels. *$P < 0.05$ and ***$P < 0.001$ from Student's *t* test. (**G**) Proportion of triads in each homoeolog expression bias category across the five homoeolog PPI groups. (**H**) Coverage of H3K36me3 (top) and H3K9ac (bottom) peaks in gene flanking regions (±5 kb) across subgenomes, normalized to subgenome averages, classified by homoeolog PPI levels. *$P < 0.05$, **$P < 0.01$, and ***$P < 0.001$ from Student's *t* test. (**I**) Browser screenshot showing asymmetrical open chromatin interactions and expression of linked genes (*TraesCS1A03G0004300*, *TraesCS1B03G0002100*, and *TraesCS1D03G0000500*). Data tracks include TAC-C peaks, loops, histone modifications, and gene transcription. (**J**) TE coverage in gene flanking regions (±5 kb) across subgenomes, normalized by the average TE coverage of singleton PPIs in A, B, and D subgenomes. (**K**) Pairwise comparisons of sequence similarity in gene flanking regions (±5 kb) across subgenomes, normalized by the average gene sequence similarity between A versus B, B versus D, and A versus D, classified by homoeolog PPI levels. *$P < 0.05$, **$P < 0.01$, and ***$P < 0.001$ from Student's *t* test.

and K). The results showed that homoeolog lacking loops exhibited higher TE coverage and lower sequence similarity in their flanking regions. This suggests that transposon insertion or sequence variation may disrupt loop structures, leading to the loss of homologous loops in specific subgenomes.

SBP and ERF family TFs occupy chromatin interaction-linked gene regulation

Chromatin conformation regulates transcription by looping TF bound CREs to the promoters of distally located target genes, as observed in mammalian cells (Fig. 5A) (*38*, *59*). To explore this mechanism in plants, we analyzed the enrichment of TFs at open chromatin interaction anchors. We found that binding sites of TFs from the V-myb avian myeloblastosis viral oncogene homolog (MYB), DNA binding with one finger (Dof), ethylene responsive factor (ERF), GATA, and SBP families were significantly enriched within the anchor regions (Fig. 5B), with SBP and ERF binding motif-enriched loops exhibiting stronger interactions compared to others (Fig. 5C).

To assess the biological significance of these TF binding site-enriched anchors, we examined their presence in functional hubs (the hubs overlapped with previously defined functional regions). Notably, 14.34% of the SBP family TF binding sites were localized in functional regulatory regions, higher than other TF families (Fig. 5D). In addition, SBP and ERF-bound functional hub anchors were linked to significantly more number of target genes compared to other hub anchors, indicating the importance of SBP and ERF targets in functional regions (Fig. 5E). Using published DAP-seq data for SBP, ERF, MYB, and Dof TF families, we found that the SBP and ERF DAP-seq peaks were more enriched in anchor regions (fig. S6A) (*60*), with SBP-bound loops showing enhanced interaction strength (fig. S6B). This suggests that SBP and ERF TFs are closely associated with chromatin interactions, emphasizing the importance of SBP-bound loops in transcriptional regulation.

Further analysis categorized genes based on SBP-associated chromatin interactions and occupancy (Fig. 5F) (*44*). Genes with SBP binding at one or both anchors (a4, a5, and a6) exhibited higher expression levels than those without SBP binding (a3) (Fig. 5F). However, basal genes not involved in chromatin interactions showed similar expression levels regardless of SBP binding (a1 and a2), indicating that chromatin loops and SBP binding synergistically enhance transcription within chromatin loop. In conclusion, we identified five TF families (MYB, Dof, ERF, GATA, and SBP) significantly enriched in open chromatin anchor regions, suggesting their roles in the formation or functional regulation of chromatin interactions.

TaSPL7/15-mediated chromatin interactions regulate photosynthesis and leaf development in wheat

Given that 48 SBP TF family members and potential functional redundancy (*61*), mutant lines with multiple SBP TF disruptions can better reveal their impact on chromatin interactions. TaSPL7 and TaSPL15 are crucial for wheat vegetative and reproductive growth (*62*). We analyzed the CRISPR/Cas9-derived knockout mutant

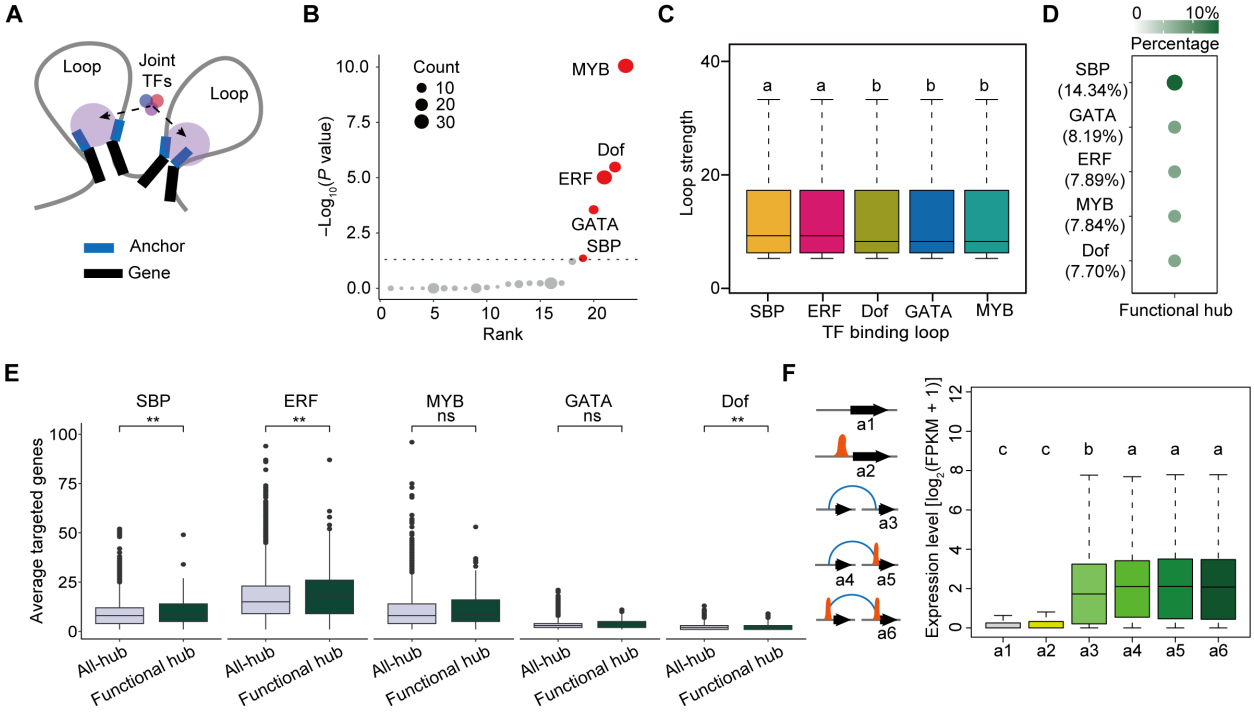

Fig. 5. Identification of TFs enriched in the chromatin interaction regions. (**A**) Schematic diagram illustrating joint TFs binding at the anchors of open chromatin interactions. (**B**) TF family enrichment analysis in hub anchor regions (two-sided Fisher's exact test). Significantly enriched TF families ($P < 0.05$) are highlighted. (**C**) Boxplot showing loop strength across five TF families. The LSD multiple comparison test was used to assess significance. Different letters denote significant differences ($P < 0.05$). (**D**) Percentage of TF binding sites enriched in functional hub anchor regions. Calculated as: TF binding sites identified in functional hubs/TF binding sites identified in all hubs. (**E**) Boxplot showing the average number of target genes (TF binding motifs in promoter regions) per hub anchor or functional hub anchor across five TF families. $^{**}P < 0.01$ from Student's *t* test. (**F**) Expression levels of genes categorized by chromatin interaction models and SBP occupancy. The LSD multiple comparison test was used to assess significance. Different letters indicate significant differences ($P < 0.05$).

Taspl7&15 (*62*) and conducted RNA sequencing (RNA-seq) on *Taspl7&15* and its wild-type (WT) counterpart, ZM7698. Transcriptomic analysis revealed strong correlations among replicates (Fig. 6A) and identified 1917 down-regulated and 1802 up-regulated genes in *Taspl7&15*. GO enrichment indicated pathways related to chloroplasts, leaf development, and carbohydrate transport were significantly affected, underscoring TaSPL7/15's role in photosynthesis and leaf development (Fig. 6B).

To investigate TaSPL7/15-mediated chromatin interactions on transcriptional regulation, we defined loops where both anchors overlapped with TaSPL7/15 DAP-seq peaks (*62*). These loop anchors were enriched for active histone marks (H3K4me3, H3K9ac, and H3K27ac) and the repressive mark H3K27me (fig. S7), suggesting potential regulation in association with multiple histone modification signals. Approximately 48% of differentially expressed genes (DEGs) were associated with TaSPL7/15-mediated loops, indicating that TaSPL7/15 maintains chromatin loops critical for gene expression (Fig. 6C and table S4). These loop-associated DEGs were significantly enriched in functional regulatory QTLs, highlighting their importance (Fig. 6D).

Key loop–associated DEGs included *chlorophyll a-b binding protein 5* (*TaLhcb5-6D*) (up-regulated), chlorophyll degradation gene *Stay-Green Rice* (*TaSGR-5D*) (down-regulated), and stomatal anion channel protein controlling stomatal closure gene *SLOW ANION CHANNEL-ASSOCIATED 1* (*TaSLAC1-D1*) (down-regulated), all influencing chlorophyll content and photosynthetic efficiency (Fig. 6E and table S5). In addition, the gene encoding transketolase (*TaTK-2D*) and the positive regulator of starch accumulation in vegetative tissues *CO_2-responsive CCT protein* (*TaNRR-A1*) were up-regulated, while the negative regulators of leaf development, such as *cytokinin oxidase/dehydrogenase 11* (*TaCKX11-A*/*B*), were down-regulated.

To validate these chromatin interactions, we focused on *TaCKX11-B*, a gene previously linked to negative regulation of leaf size and photosynthetic efficiency in rice and wheat (*63*). A 57-kb upstream interaction loop was identified in WT (ZM7698) but lost in *Taspl7&15* (Fig. 6F). TAC-C–quantitative PCR (qPCR) confirmed the loss of this interaction loop in *Taspl7&15* (*CR127*) (Fig. 6G, top), and reverse transcription (RT)–qPCR demonstrated reduced *TaCKX11-B* expression (Fig. 6G, bottom). Luciferase reporter assays validated the enhancer-like function of the distal region on *TaCKX11-B* (Fig. 6H). Similar loop disruption was observed for *TaSGR-5D*, *TaNRR-A1*, and *TaTK-2D* (fig. S8, A to C).

Phenotypic analysis showed *Taspl7&15* mutants had larger leaf size, higher chlorophyll content, and improved photosynthetic efficiency (Fig. 6, I and J). Liquid chromatography–mass spectrometry (LC-QQQ-MS) analysis revealed increased levels of photosynthetic intermediates, including pentose phosphate (D-ribose 5-phosphate (R5P), ribulose-5-phosphate (Ru5P), D-xylulose-5-phosphate (Xu5P), and D-sedoheptulose-7-phosphate (S7P) in *Taspl7&15* compared to ZM7698 (fig. S9), indicating enhanced photosynthetic capacity. Notably, the absence of phosphoglycerate 3-phosphoglycerate (3PGA) and 2-phosphoglycerate (2PGA) suggested reduced photorespiratory flux, potentially boosting photosynthetic efficiency (fig. S9). Moreover, we observed larger starch granules in *Taspl7&15′* leaves than in those of ZM7698 (Fig. 6K). Those phenotypic data fit well with the observed transcriptional change of above-mentioned genes in *Taspl7&15*.

In summary, TaSPL7/15 mediates chromatin interactions critical for regulating photosynthesis-related genes and leaf development. Loss of TaSPL7/15 disrupts these loops, altering gene expression and enhancing photosynthetic efficiency in wheat leaves.

DISCUSSION

Understanding the spatial organization of CREs is essential for deciphering gene regulation (*64*), particularly in complex genomes such as wheat, a hexaploid species (*29*). The 3D structure of the genome plays a crucial role in how CREs, such as enhancers, interact with their target genes to control key biological processes (*42*, *44*). Traditional methods such as Hi-C, HiChIP, and OCEAN-C have advanced our understanding of chromatin interactions but have been less effective in capturing the fine-scale interactions between CREs and genes in wheat (*25*, *28*, *30*).

TAC-C: A plant specialized fine-scale 3D chromatin organization study tool

Because of the higher spatial resolution of ATAC-seq compared to FAIRE-seq (*27*), we developed the TAC-C method by integrating ATAC-seq with in situ Hi-C, facilitating targeted capture of interactions within open chromatin regions. This advancement not only heightens spatial resolution but also reduces the sequencing depth required to yield meaningful data. This innovation holds particular significance for cost reduction, especially in the context of crops with large genomes such as wheat. TAC-C excels in identifying active CREs and demonstrates better overlap with epigenetic modifications compared to other methods (Fig. 1). Using wheat as a model, TAC-C has proven its robustness in capturing intricate details of chromatin interactions that are crucial for understanding gene regulation in large-genome species. The method's adaptation for plant samples, particularly those rich in sugars and polyphenols, further underscores its versatility and reliability. Unlike the recently developed ChIATAC technique (*18*), TAC-C omits the use of SDS in nuclei treatment (Fig. 1). SDS as a surfactant has the potential to disrupt the binding between histones and DNA. This disruption facilitates Tn5 accessibility to closed chromatin regions. Consequently, compared to the ChIATAC, TAC-C is more similar to ATAC-seq. Moreover, ChIATAC was only used in animal cells, with no reported application in plants, while TAC-C is a technology tailored specifically for plant systems. These makes TAC-C not only a powerful alternative but also a more specialized tool for studying the 3D genome organization in plants. The success of TAC-C in rice, wheat, maize, sorghum (Fig. 2) suggests its potential applicability across other complex genomes, providing a previously unexplored avenue to explore the spatial organization and regulatory mechanisms underlying large-genome species.

Conservation and biological importance of TAC-C identified chromatin interaction hub anchors

TAC-C identifies open chromatin regions frequently interacting with other regions, termed hub anchors (Fig. 2). Across different crops species, hub anchors exhibit common features such as low-frequency base variations and higher expression levels of their associated node genes (Fig. 2). Moreover, a significant overlap was observed between previously reported QTL, eQTL, and breeding selection intervals with chromatin interaction anchors, especially hub anchors (Fig. 3). This underscores the functional importance of open chromatin interactions in regulating agronomic traits. GWAS has identified numerous QTLs in crops with large genomes such as maize and wheat (*65*, *66*), often located in intergenic regions, complicating their functional interpretation. Chromatin interactions can be used as physical evidence to connect GWAS-identified SNPs to their target genes, offering insights into trait-associated elements.

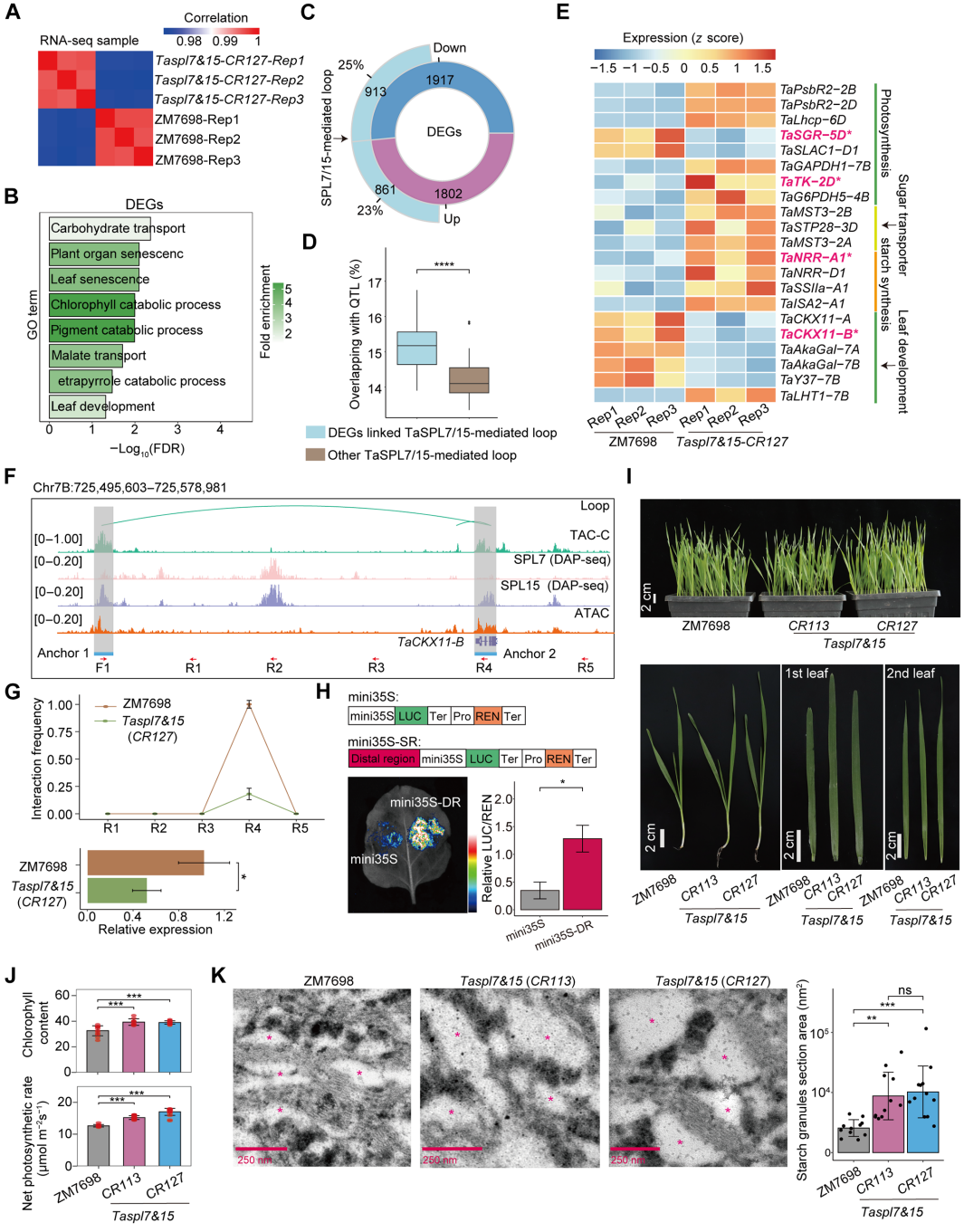

Fig. 6. SPL-associated chromatin interactions in regulating photosynthetic energy metabolism. (**A**) Clustering of samples for RNA-seq according to the Pearson's correlation coefficient of gene expression levels. (**B**) GO enrichment analysis of DEGs in *Taspl7&15* versus ZM7698. (**C**) Proportion of DEGs overlapped with TaSPL7/15-mediated chromatin loop–linked genes. (**D**) Percentage of overlapped interactions between TaSPL7/15-mediated loop linked DEGs and other TaSPL7/15-mediated loop. ***$P < 0.001$ from Student's *t* test. (**E**) Expression of key genes involved in photosynthesis and leaf development. Expression levels were normalized by *z* score. The genes that are further validated in the following are highlighted. (**F**) Chromatin interactions of *TaCKX11-B*. Profiles of TaSPL7/15 DAP-seq, ATAC, and chromatin interactions around *TaCKX11-B* and its distal regulatory site are shown, with anchor regions highlighted. The bottom panel shows the locations of primer in TAC-C–qPCR experiments. (**G**) Quantitative relative interacting frequency of loop regions determined by TAC-C-qPCR in ZM7698 and *Taspl7&15* (*CR127*) (top). The quantitative relative expression of *TaCKX11-B* by RT-qPCR assay in ZM7698 and *Taspl7&15* (*CR127*) (bottom). Error bars: ±SD $n = 3$, *$P < 0.05$ from Student's *t* test. (**H**) Luciferase reporter assay validating the transcriptional regulatory role of the distal regions (DRs) on *TaCKX11-B*. The distal anchor sequence was introduced into the proximal region of the *TaCKX11-B* promoter. *$P < 0.05$ from Student's *t* test. (**I**) Phenotypes of leaves of the wheat accession ZM7698 and two CRISPR-generated *Taspl7&15* mutant lines. (**J**) Chlorophyll content and net assimilation rates of carbon dioxide between ZM7698 and the two CRISPR lines of *Taspl7&15* mutant at the seedling stage. ***$P < 0.001$ from Student's *t* test. (**K**) Transmission electron microscopy images of chloroplasts of for ZM7698 and *Taspl7&15* two mutant lines. Red asterisks indicate starch granules. The area of the starch granules section is calculated by ImageJ. **$P < 0.01$, ***$P < 0.001$ and ****$P < 0.0001$ from Student's *t* test. FDR, false discovery rate.

For example, our study revealed chromatin interactions between *TaNAL1-5A-like* and its eQTL loci (Fig. 3). This research advances our understanding and paves the way for precision breeding using advanced editing technique.

Chromatin spatial organization contributes to subgenome gene expression bias

Previous research has demonstrated that differences in epigenetic modifications, transposon insertions, and TF binding motifs significantly influence homoeolog expression bias in wheat (*41*, *58*, *67*, *68*). Our TAC-C data support these findings, revealing extensive subgenome-specific PPIs (Fig. 4). Notably, the D subgenome exhibited more chromatin interactions compared to the A and B subgenomes (Fig. 4), possibly due to the latter undergoing epigenetic homogenization over time (*69*). In contrast, the D subgenome, with its shorter evolutionary history, may retain more diploid-like epigenetic features.

Our results also show an enrichment of transposons in subgenome-specific interaction anchors (Fig. 4), suggesting that some transposons have evolved into regulatory elements, influencing subgenome-specific gene expression through chromatin looping (*60*, *68*, *70*). While previous studies focused on genetic sequence variations and epigenetic modifications (*41*, *60*, *71*), our research highlights the importance of distal chromatin interactions in shaping subgenome bias (Fig. 4). Contrary to earlier reports suggesting that chromatin interaction divergence does not contribute to homoeolog gene expression bias (*28*), we observed that homoeolog pairs losing open chromatin loops exhibit significantly lower expression levels in the affected subgenome. This discrepancy may stem from TAC-C's higher precision and resolution, allowing the detection of subtle imbalances in chromatin loops even when open chromatin remain unchanged. We propose that sequence variations and transposon insertions near homologous genes reshape the chromatin landscape including asymmetric chromatin interactions, driving biased gene expression and reinforcing subgenome asymmetry in hexaploid wheat.

SBPs in chromatin organization and wheat development

While CTCF/cohesin complexes control chromatin loops in animals (*35*, *36*), and TCPs shape chromatin structure in *Marchantia* (*40*), the processes governing chromatin loops in higher plants such as wheat are not well understood (*72*). TaSPL7/15 participate in wheat vernalization process by directly anchoring the *VERNALIZATION1* (*VRN1*) promoter and 30-kb upstream regulatory elements of *VRN3* (*73*), yet their broader role in wheat 3D chromatin structure has been unexplored. Our findings reveal an enrichment of SBP and ERF TF binding motifs in chromatin's open anchor regions (Fig. 5), indicating the potential role in maintaining wheat chromatin organization. In *Taspl7&15* mutants, a substantial overlap was observed between DEGs and TaSPL7/15-mediated loop linked genes (Fig. 6), particularly those involved in photosynthesis, starch synthesis, sugar transport, and leaf development (Fig. 6), leading to increased photosynthetic efficiency in *Taspl7&15*. Specifically, the loss of distal regulatory interaction for *TaCKX11-A*, *TaCKX11-A*, *TaSGR-5D*, *TaTK-2D*, and *TaISA2* resulted in longer leaves, reduced chlorophyll degradation, enhanced photosynthesis efficiency, and increased photosynthetic products (Fig. 6). In addition, SPLs are quantitatively regulated by miRNA156s, conserved microRNAs associated with plant developmental ages across species (*74*, *75*), suggesting that 3D chromatin organization may undergo SPL-mediated change as plants mature, contributing to developmental morphology.

MATERIALS AND METHODS

Plant materials and growth conditions

The *O. sativa*, *S. bicolor*, *Z. mays*, and *T. aestivum* (Chinese Spring) were used in this study. The *Taspl7&15* CRISPR lines were obtained from a previous study (*62*). The seeds were surface sterilized in 2% NaClO for 20 min and then rinsed overnight with flowing water. The seeds were germinated and then transferred to soil and grown in the greenhouse at 22°C/20°C day/night, under long day conditions (16-hour light/8-hour dark). When the material grows to one leaf and one heart period, the leaves were sampled for the RNA-seq (three replicates) and TAC-C experiments (two replicates).

TAC-C library construction

TAC-C experiments require three processions, including: Plant tissue was cut into approximately 0.5 cm^2 pieces and then fixed using nuclei isolation buffer (NIB) containing 4% formaldehyde [20 mM Hepes, 250 mM sucrose, 1 mM $MgCl_2$, 5 mM KCl, 1 mM dithiothreitol (DTT), 1% protease inhibitor cocktail for plants, 0.25% Triton X-100, 40% glycerol, and 4% formaldehyde]. The reaction was quenched by adding 0.125 M glycine and incubated on ice for 15 min. The fixed plant tissue was washed three times with NIB (20 mM Hepes, 250 mM sucrose, 1 mM $MgCl_2$, 5 mM KCl, 1 mM DTT, 1% protease inhibitor cocktail for plants, 0.25% Triton X-100, and 40% glycerol). After removing excess liquid from the surface using absorbent paper, nuclear extraction could be performed directly or the samples could be stored at −80°C.

The processed plant tissue, subjected to liquid nitrogen grinding, was transferred to a 15-ml tube, and the pellets were then resuspended using NIB. The suspension was incubated with shaking on ice for 10 min. Subsequently, the suspension was successively filtered through 10 and 40-μm strainers, followed by centrifugation at 1260*g* at 4°C for 5 min. After discarding the supernatant, the pellets were washed twice with NIB and then washed twice with 1.2× NEBuffer r2.1 (NEB, B6002S). Nuclei were obtained after centrifugation at 1260*g* at 4°C for 5 min with the removal of the supernatant. The isolated nuclei can be used for TAC-C library preparation or stored at −80°C.

Using 10,000 to 50,000 nuclei as the starting material for TAC-C library construction, the nuclei were resuspended in 500 μl 1.2× NEBuffer r2.1, and 40 μl of Dpn II (NEB, R0543L) was added. The reaction was carried out overnight at 37°C with constant agitation at 900 rpm in a metal bath. Subsequently, the reaction was terminated by incubating at 65°C for 20 min.

After that, 37.5 μl of Biotin-14-dCTP (Invitrogen, 19518018), 1.5 μl of 10 mM 2′-deoxyadenosine 5′-triphosphate (NEB, N0446S), 1.5 μl 10 mM 3′-deoxythymidine 5′-triphosphate (NEB, N0446S), 1.5 μl of 10 mM 2′-deoxyguanosine 5′-triphosphate (NEB, N0446S), and 10 μl of DNA polymerase I, large (Klenow) fragment (NEB, M0210L) were added, and the reaction was carried out at 37°C for 1 hour in a metal bath to complete biotin labeling. Following this, 598 μl of 2× rapid ligation buffer and 6 μl of T4 DNA ligase (Enzymatics, L6030-HC-L) were added, and the reaction was carried out at 20°C for 4 hours to complete the in situ ligation. The reaction mixture was centrifuged at 5000*g* for 5 min, the supernatant was discarded, and the nuclear pellet was resuspended in TE buffer (pH 10; Invitrogen, AM9858) and incubated at 70°C for 1 hour. The reaction mixture was centrifuged at 1000*g* for 5 min, and 1 μl of exonuclease III (NEB, M0206), 10 μl of 10× NEBuffer1 (NEB, M0206), and 89 μl of nuclease-free water were added. The reaction was carried out at 37°C for 20 min, followed by 72°C for 30 min to terminate the reaction.

After washing once with 500 μl of 1× TD buffer [10 mM tris-HCl (pH 7.4), 5 mM $MgCl_2$, and 0.25% dimethyl formamide], the samples were centrifuged at 1260*g* for 5 min, and the supernatant was discarded. Then, 50 μl of 2 × TD buffer [20 mM tris-HCl (pH 7.4), 10 mM $MgCl_2$, and 0.5% dimethyl formamide] and 8 μl of TTE Mix V50 (Vazyme, TD711-02), 42 μl of nuclease-free water were added, and the reaction was carried out at 900 rpm, 37°C for 1 hour in a metal bath.

After the reaction, the DNA was purified using the MinElute PCR Purification Kit (QIAGEN, 28004), washed with 100 μl of buffer EB (QIAGEN, 19086), and then incubated with 40 μl of Dynabeads MyOne Streptavidin C1 (Invitrogen, 65001) at room temperature for 20 min. The beads were washed twice with binding and washing buffer [5 mM tris-HCl (pH 7.5), 0.5 mM EDTA, and 1 M NaCl].

Last, the DNA was amplified by adding 50 μl of TruePrep CUT&Tag Amplification Mix (Vazyme, TD612-01), 40 μl of nuclease-free water, 5 μl of 20 μM N7 index primer (TGTGAGCCAAGGAGTTGTTGTCTTCNNNNNNNNNNGTCTCGTGGGCTCGG), and 5 μl of 20 μM N5 primer (/5Phos/GAACGACATGGCTACGATCCGACTTTCGTCGGCAGCGTC). The amplification conditions were as follows: 72°C for 5 min, 98°C for 30 s; 98°C for 10 s, 63°C for 30 s, 72°C for 1 min, 10 cycles; 72°C for 5 min; hold at 4°C. The PCR products were purified using 60 μl of Ampure beads (Beckman Coulter, A63881), incubated for 5 min, and placed on a magnetic stand for 5 min, and then the supernatant was transferred to a new 1.5-ml tube. After incubating with 20 μl of Ampure beads for 5 min and placing on a magnetic stand for 5 min, the supernatant was discarded. The beads were washed twice with 80% ethanol, and after the beads were air-dried, the DNA was recovered using buffer EB. This is the TAC-C library. The TAC-C library was sequenced using MGI 2000 (2 × 100 base pair). The relevant chemicals and enzymes are listed in table S6. For parallel control, Dpn II was replaced by BSA while keeping all other steps unchanged.

TAC-C data processing

Initially, the raw reads underwent trimming using the hicup_truncater v0.5.9 tool (*76*) to identify and eliminate the ligated junction points within the reads, specifically removing the sequences after the recognition site of restriction enzyme. Subsequently, the trimmed reads were mapped to the reference genome: *S. bicolor* (*77*), *Z. mays* (*78*), *O. sativa* (*79*), and *T. aestivum* (*80*) through the bwa v0.7.17 software (*81*), with reads having a mapping quality (MAPQ) score < 1 being discarded to ensure mapping accuracy. The Hi-C-Pro v2.10.0 (*82*) tool was used to filter out dangling end pairs, Re-ligation Pairs, Self-cycle Pairs, and Dumped Pairs. Following the removal of PCR duplicates, the remaining valid read pairs were used for calling peaks and loops. The calling of peaks from the remaining valid read pairs was performed using MACS2 (*83*) the parameter "-q 0.01 -f BAM --nomodel --extsize 150 --shift -75 --call-summits --nolambda", The overlapping peaks between two biological replicates were used as an anchor to identify open chromatin interactions by hichipper (https://github.com/aryeelab/hichipper) with default setting in two biological replicates. Finally, the intrachromosomal loop from two biological replicates were merged by hicMergeLoops from HiCExplorer software (*84*) with the parameter "-r 10000." TAC-C interaction heatmaps were produced with HiCPlotter v0.8.1 at 1-Mb resolution (*85*).

ATAC-seq, OCEAN-C, and Hi-C data processing

ATAC-seq experiments followed the previously described method (*32*). Tn5 transposase used and tagmentation assay are done following the manual (Vazyme, TD501-01). Libraries were purified with AMPure beads (Beckman, A63881) and sequenced using the Illumina NovaSeq platform at Annoroad Gene Technology. Data processing and reads alignment were performed as previously described (*32*). MACS2 v2.1.4 was used to call peaks. Parameters were the same as TAC-C data processing.

We downloaded the OCEAN-C and Hi-C data of Chinese Spring from the NGDC BioProject database (accession number CRA003731) and National Center for Biotechnology Information (NCBI) (accession number GSE133885) (*25*, *28*). Reads were aligned to the International Wheat Genome Sequencing Consortium (IWGSC) RefSeq v2.1 reference genome. The data analysis procedures are the same with the analysis for TAC-C data. In particular, for the Hi-C intrachromosomal loops, we directly use the published results of previous study (*30*).

RNA-seq and RNA-seq data analysis

Total RNA was extracted using the HiPure Plant RNA Mini Kit according to the manufacturer's instructions (Magen, R4111-02). RNA-seq libraries' construction and sequencing platform were the same as previous description (*32*) by Annoroad Gene Technology.

Low-quality reads and adapter sequences were removed using Cutadapt (*86*) and Trimmomatic (*87*), respectively. Retained clean RNA-seq reads were mapped to the same version reference genome with TAC-C by using STAR (*88*) (version 2.5.4b) with default parameters (SortedByCoordinate --quantMode TranscriptomeSAM GeneCounts), and accurate transcript was quantified using RSEM (*89*) (version 1.3.0). In addition, RSEM was also used to analyze the mRNA expression level by calculating fragments per kilobase of exon model per million mapped reads. The RNA-seq reads counts of DEGs were filtered with $|\log_2(\text{fold change})| > 0$ and false discovery rate < 0.05 by using R packages edgeR (*90*).

GO analysis

The GO functional enrichment was performed using the find_enrichment.py from goatools software (*91*).

ChIP-seq data analysis

Sequencing reads of H3K4me3, H3K9ac, H3K27ac, H3K27me3, H3K9me3, and H3K36me3 of Chinese Spring were obtained from previous study (*41*). ChIP-seq data are available in NCBI GEO under accession number GSE121903. Sequencing reads were cleaned by removing bases that had low quality scores (<20) and removing sequencing adaptors by Cutadapt (*86*) and filtering out short reads by Trimmomatic (*87*). The reads of ChIP-seq were mapped to the IWGSC RefSeq v2.1 reference genome using Bowtie2 (*92*) with default setting. The concordantly mapped reads (MAPQ > 10) were kept and PCR duplication was further removed with Picard (https://broadinstitute.github.io/picard/). Peaks of ChIP-seq libraries were detected using MACS2 (2.1.2) with the parameter "-f BAM –nomodel -q 0.05."

DAP-seq data analysis

For SPL7A, SPL7B, SPL7D, SPL15A, SPL15B, and SPL15D DAP-seq data analysis, the raw sequencing reads (from the NCBI accession

number PRJNA779959) (*62*) were cleaned by removing bases that had low-quality scores (<20) and removing sequencing adaptors by Cutadapt (*86*) and filtering out short reads by Trimmomatic (*87*). As a result, about 5 million reads with a MAPQ score > 20 was obtained for further analyses. The cleaned reads were mapped to the IWGSC RefSeq v2.1 reference genome using Bowtie2 (*92*) (version 2.4.4) with default settings. MACS2 (*83*) was used for peak calling of the ChIP-seq datasets, with options: -g 7.83e8 --call-summits --bdg -q 0.01 --nomodel. Typical DAP-seq loci were plotted using Integrative Genomics Viewer (IGV) solftware (*93*).

ERF, Dof, MYB, and other SPL DAP-seq peak were download from GSE192815 and GSE188699 (*60*, *62*, *68*). The overlap of DAP-seq peak with anchor was calculated using BEDTools (*94*) with parameter: intersect -wa -wb.

Identification of homoeolog PPIs

High-confidence gene models from the IWGSC (version 1.0) were used for defining triad genes. Homolog genes between each pair of A, B, and D subgenomes were identified as previously described (*58*). The gene ID from IWGSC (version 1.0) were converted to IWGSC (version 2.1) by TriticeaeGeneTribe (TGT) (http://wheat.cau.edu.cn/TGT/) (*95*). Then, a total 18,333 homoeolog groups with only one gene copy in each subgenome were defined as triads. PPIs whose anchors on one side were homoeolog genes between A, B, and D subgenomes and anchors on another side were also homoeolog genes were defined as homoeolog PPIs, and the corresponding genes are defined as homoeolog PPI genes.

TF motif analysis

We use Homer (*96*) to find enrichment of sequence motifs with default parameters. Sequences in TAC-C anchor in were used as input. The "Known Results" were used as final results. The enriched TF motifs were further used for TF family enrichment analysis. Enrichment analysis was done using the R package clusterProlifer (v3.16.1) (*97*), with a threshold $P_{adj} < 0.05$. The set of 1007 "known TF motifs" from Homer served as the background, and enrichment was calculated by enricher function.

RT-qPCR and TAC-C-qPCR

Total RNA was extracted using the HiPure Plant RNA Mini Kit according to the manufacturer's instructions (Magen, R4111-02). First-strand cDNA was synthesized from 2 μg of DNase I–treated total RNA using the TransScript First Strand cDNA Synthesis SuperMix Kit (TransGen, AT301-02). RT-qPCR was performed using the ChamQ Universal SYBR qPCR Master Mix (Vazyme, Q711-02) by QuantStudio5 (Applied Biosystems). The expression of interested genes was normalized to tubulin for calibration, and the relative expression level is calculated via the $2^{-\Delta\Delta CT}$ analysis method (*98*). Primers used for RT-qPCR are listed in table S7.

To calculate the relative interaction frequencies between two candidate regions, we used the TAC-C-qPCR method. TAC-C library DNA serves as the template, with specific primer pairs designed to flank predicted loop anchors, and additional primers placed left and right of the predicted anchors. Quantitative PCR is used to detect the enrichment of fragment interactions in the biotin-labeled TAC-C library. If interactions exist, then enrichment will occur in the TAC-C library, allowing the specific primer pairs to amplify PCR products. In the absence of interactions, the primer pairs will not yield PCR products. The higher the degree of enrichment indicates the higher the frequency of loop interactions. For example, primers were designed for an internal control region of the *TaCKX11-B* genomic locus that was not subjected to Dpn II digestion to normalize the DNA concentrations across different samples. Upon completion of the qPCR experiments using this method, we were able to more accurately analyze and quantify the interaction frequencies between the candidate regions. The relevant primer information is listed in table S7.

Luciferase reporter assay

To generate the p*TaNAL1-like-5A:LUC* construct, we amplified 3-kb promoter fragments upstream of *TaNAL1-like-5A* from Chinese Spring (CS) and ligated them with the transient expression vector CP461-LUC (Luciferase), which was constructed as the reporter vector. The p35S-*Traes5A02G000700*-GFP (green fluorescent protein) construct was used as effector. Then, p*TaNAL1-like-5A:LUC* and p35S:*Traes5A02G000700-GFP* were transformed into *Agrobacterium tumefaciens* strain GV3101. The p*TaNAL1-like-5A:LUC* and p35S-pro:GFP were cotransformed as controls.

To generate *PR*-mini*35S-pro:LUC* construct, the genomic sequence of distal regulatory region was amplified and fused in-frame with the pMY155-mini35S vector to generate the reporter construct. Then, *mini35S-pro:LUC* (as control) and *PR-mini35S-pro:LUC* were transformed into *A. tumefaciens* strain *GV3101*.

Then, these strains were injected into *Nicotiana benthamiana* leaves (six to eight leaf stage) in different combinations with p19, which was used to suppress RNA silencing. Dual luciferase assay reagents (Promega, VPE1910) with the *Renilla* luciferase gene as an internal control were used for luciferase imaging. The Dual-Luciferase Reporter Assay System Kit (Promega, E2940) was used to quantify fluorescence signals. Relative LUC activity was calculated by the ratio of LUC/REN. The relevant primers are listed in table S7.

Measurement of photosynthetic capacity, chlorophyll content, and leaf area

The measurement of photosynthetic capacity was conducted on the *Taspl7&15-CR* lines. The penultimate new leaves fully expanded were selected for the measurement of net photosynthesis rate with a portable gas exchange and fluorescence system (GFS-3000, Walz, Germany). The environmental parameters were set as follows: an air flow of 400 mmol s^{-1} through the chamber, a leaf temperature of 25°C, and a CO_2 concentration of 400 μmol mol^{-1}.

Chlorophyll content was measured with the same penultimate new fully expanded leaves at room temperature with a TYS-B Chlorophyll meter (Zhejiang TP, China). Leaf area was measured with the same penultimate new fully expanded leaves at room temperature with a Yaxin-1241 portable leaf area meter (Beijing Yaxinliyi Science and Technology Co. Ltd., China).

LC-MS analysis

The endogenous levels of R5P/Ru5P/Xu5P, 3PGA/2PGA, E4P, DHPA, S7P, F6P/G1P, and G6P were determined with an ultraperformance liquid chromatography tandem mass spectrometry analytical platform consisting of an Agilent 1290 Infinity liquid chromatography pump and a 6495 triple quadrupole mass spectrometer (Agilent Technology Co. Ltd., America), following the protocol described in previous study (*99*).

Ultrathin sections and scanning electron microscopy

Ultrathin (70 nm) sections of ZM7698 and *Taspl7&15-CR* leaves were prepared using a Leica EM UC7 ultramicrotome (Leica, Vienna,

Austria), as previously described (*100*). Sections were placed on formvar-coated copper grids and poststained with uranyl acetate and lead citrate and observed under a HT-7700 transmission electron microscope (Hitachi, Tokyo, Japan) operated at 80 kV.

Statistics and data visualization

If not specified, then R (https://cran.r-project.org/; version 4.3.2) was used to compute statistics and generate plots. For the two groups' comparison of data, the Student's *t* test was used such as Figs. 2, 3, 4, 5, and 6, and figs. S1, S3, S5, and S6. For three or more independent groups comparison of data, Fisher's least significant difference was used, such as Figs. 3B and 5 (C and F). Pearson's correlation was used in figs. S1A and S3H. For enrichment analysis, Fisher's exact test was used, such as Figs. 5B and 6B, and fig. S5, C and D. The IGV was used for the visual exploration of genomic data, such as Figs. 1I, 3F, 4I, and 6F, and figs. S5H and S8 (A to C)

Supplementary Materials

The PDF file includes:
Figs. S1 to S9
Legends for tables S1 to S7

Other Supplementary Material for this manuscript includes the following:
Tables S1 to S7

REFERENCES AND NOTES

1. A. Hendelman, S. Zebell, D. Rodriguez-Leal, N. Dukler, G. Robitaille, X. Wu, J. Kostyun, L. Tal, P. Wang, M. E. Bartlett, Y. Eshed, I. Efroni, Z. B. Lippman, Conserved pleiotropy of an ancient plant homeobox gene uncovered by cis-regulatory dissection. *Cell* **184**, 1724–1739.e16 (2021).
2. R. J. Schmitz, E. Grotewold, M. Stam, Cis-regulatory sequences in plants: Their importance, discovery, and future challenges. *Plant Cell* **34**, 718–741 (2022).
3. A. P. Marand, A. L. Eveland, K. Kaufmann, N. M. Springer, *cis*-Regulatory elements in plant development, adaptation, and evolution. *Annu. Rev. Plant Biol.* **74**, 111–137 (2023).
4. X. Lin, Y. Xu, D. Wang, Y. Yang, X. Zhang, X. Bie, L. Gui, Z. Chen, Y. Ding, L. Mao, X. Zhang, F. Lu, X. Zhang, C. Uauy, X. Fu, J. Xiao, Systematic identification of wheat spike developmental regulators by integrated multi-omics, transcriptional network, GWAS, and genetic analyses. *Mol. Plant* **17**, 438–459 (2024).
5. X. Bai, Y. Huang, Y. Hu, H. Liu, B. Zhang, C. Smaczniak, G. Hu, Z. Han, Y. Xing, Duplication of an upstream silencer of FZP increases grain yield in rice. *Nat. Plants* **3**, 885–893 (2017).
6. R. M. Clark, T. N. Wagler, P. Quijada, J. Doebley, A distant upstream enhancer at the maize domestication gene tb1 has pleiotropic effects on plant and inflorescent architecture. *Nat. Genet.* **38**, 594–597 (2006).
7. J. O. Melo, L. G. C. Martins, B. A. Barros, M. R. Pimenta, U. G. P. Lana, C. E. M. Duarte, M. M. Pastina, C. T. Guimaraes, R. E. Schaffert, L. V. Kochian, E. P. B. Fontes, J. V. Magalhaes, Repeat variants for the SbMATE transporter protect sorghum roots from aluminum toxicity by transcriptional interplay in cis and trans. *Proc. Natl. Acad. Sci. U.S.A.* **116**, 313–318 (2019).
8. S. L. Klemm, Z. Shipony, W. J. Greenleaf, Chromatin accessibility and the regulatory epigenome. *Nat. Rev. Genet.* **20**, 207–220 (2019).
9. G. E. Crawford, I. E. Holt, J. Whittle, B. D. Webb, D. Tai, S. Davis, E. H. Margulies, Y. Chen, J. A. Bernat, D. Ginsburg, D. Zhou, S. Luo, T. J. Vasicek, M. J. Daly, T. G. Wolfsberg, F. S. Collins, Genome-wide mapping of DNase hypersensitive sites using massively parallel signature sequencing (MPSS). *Genome Res.* **16**, 123–131 (2006).
10. P. G. Giresi, J. Kim, R. M. McDaniell, V. R. Iyer, J. D. Lieb, FAIRE (Formaldehyde-Assisted Isolation of Regulatory Elements) isolates active regulatory elements from human chromatin. *Genome Res.* **17**, 877–885 (2007).
11. J. D. Buenrostro, P. G. Giresi, L. C. Zaba, H. Y. Chang, W. J. Greenleaf, Transposition of native chromatin for fast and sensitive epigenomic profiling of open chromatin, DNA-binding proteins and nucleosome position. *Nat. Methods* **10**, 1213–1218 (2013).
12. Z. Lu, A. P. Marand, W. A. Ricci, C. L. Ethridge, X. Zhang, R. J. Schmitz, The prevalence, evolution and chromatin signatures of plant regulatory elements. *Nat. Plants* **5**, 1250–1259 (2019).
13. E. Calo, J. Wysocka, Modification of enhancer chromatin: What, how, and why? *Mol. Cell* **49**, 825–837 (2013).
14. M. J. Fullwood, C. L. Wei, E. T. Liu, Y. Ruan, Next-generation DNA sequencing of paired-end tags (PET) for transcriptome and genome analyses. *Genome Res.* **19**, 521–532 (2009).
15. E. Lieberman-Aiden, N. L. van Berkum, L. Williams, M. Imakaev, T. Ragoczy, A. Telling, I. Amit, B. R. Lajoie, P. J. Sabo, M. O. Dorschner, R. Sandstrom, B. Bernstein, M. A. Bender, M. Groudine, A. Gnirke, J. Stamatoyannopoulos, L. A. Mirny, E. S. Lander, J. Dekker, Comprehensive mapping of long-range interactions reveals folding principles of the human genome. *Science* **326**, 289–293 (2009).
16. T. Li, L. Jia, Y. Cao, Q. Chen, C. Li, OCEAN-C: Mapping hubs of open chromatin interactions across the genome reveals gene regulatory networks. *Genome Biol.* **19**, 54 (2018).
17. M. R. Mumbach, A. J. Rubin, R. A. Flynn, C. Dai, P. A. Khavari, W. J. Greenleaf, H. Y. Chang, HiChIP: Efficient and sensitive analysis of protein-directed genome architecture. *Nat. Methods* **13**, 919–922 (2016).
18. H. Chai, H. Tjong, P. Li, W. Liao, P. Wang, C. H. Wong, C. Y. Ngan, W. J. Leonard, C.-L. Wei, Y. Ruan, ChIATAC is an efficient strategy for multi-omics mapping of 3D epigenomes from low-cell inputs. *Nat. Commun.* **14**, 213 (2023).
19. M. Louwers, R. Bader, M. Haring, R. van Driel, W. de Laat, M. Stam, Tissue- and expression level-specific chromatin looping at maize *b1* epialleles. *Plant Cell* **21**, 832–842 (2009).
20. L. Zhao, S. Wang, Z. Cao, W. Ouyang, Q. Zhang, L. Xie, R. Zheng, M. Guo, M. Ma, Z. Hu, W. K. Sung, Q. Zhang, G. Li, X. Li, Chromatin loops associated with active genes and heterochromatin shape rice genome architecture for transcriptional regulation. *Nat. Commun.* **10**, 3640 (2019).
21. T. Misteli, Beyond the sequence: cellular organization of genome function. *Cell* **128**, 787–800 (2007).
22. A. Göndör, R. Ohlsson, Enhancer functions in three dimensions: Beyond the flat world perspective. *F1000Res* **7**, 681 (2018).
23. A. Salman-Minkov, N. Sabath, I. Mayrose, Whole-genome duplication as a key factor in crop domestication. *Nat. Plants* **2**, 16115 (2016).
24. M. Wang, P. Wang, M. Lin, Z. Ye, G. Li, L. Tu, C. Shen, J. Li, Q. Yang, X. Zhang, Evolutionary dynamics of 3D genome architecture following polyploidization in cotton. *Nat. Plants* **4**, 90–97 (2018).
25. L. Concia, A. Veluchamy, J. S. Ramirez-Prado, A. Martin-Ramirez, Y. Huang, M. Perez, S. Domenichini, N. Y. Rodriguez Granados, S. Kim, T. Blein, S. Duncan, C. Pichot, D. Manza-Mianza, C. Juery, E. Paux, G. Moore, H. Hirt, C. Bergounioux, M. Crespi, M. M. Mahfouz, A. Bendahmane, C. Liu, A. Hall, C. Raynaud, D. Latrasse, M. Benhamed, Wheat chromatin architecture is organized in genome territories and transcription factories. *Genome Biol.* **21**, 104 (2020).
26. S. S. Rao, M. H. Huntley, N. C. Durand, E. K. Stamenova, I. D. Bochkov, J. T. Robinson, A. L. Sanborn, I. Machol, A. D. Omer, E. S. Lander, E. L. Aiden, A 3D map of the human genome at kilobase resolution reveals principles of chromatin looping. *Cell* **159**, 1665–1680 (2014).
27. K. Davie, J. Jacobs, M. Atkins, D. Potier, V. Christiaens, G. Halder, S. Aerts, Discovery of transcription factors and regulatory regions driving in vivo tumor development by ATAC-seq and FAIRE-seq open chromatin profiling. *PLOS Genet.* **11**, e1004994 (2015).
28. J. Yuan, H. Sun, Y. Wang, L. Li, S. Chen, W. Jiao, G. Jia, L. Wang, J. Mao, Z. Ni, X. Wang, Q. Song, Open chromatin interaction maps reveal functional regulatory elements and chromatin architecture variations during wheat evolution. *Genome Biol.* **23**, 34 (2022).
29. The International Wheat Genome Sequencing Consortium (IWGSC), R. Appels, K. Eversole, N. Stein, C. Feuillet, B. Keller, J. Rogers, C. J. Pozniak, F. Choulet, A. Distelfeld, J. Poland, G. Ronen, A. G. Sharpe, O. Barad, K. Baruch, G. Keeble-Gagnère, M. Mascher, G. Ben-Zvi, A.-A. Josselin, A. Himmelbach, F. Balfourier, J. Gutierrez-Gonzalez, M. Hayden, C. Koh, G. Muehlbauer, R. K. Pasam, E. Paux, P. Rigault, J. Tibbits, V. Tiwari, M. Spannagl, D. Lang, H. Gundlach, G. Haberer, K. F. X. Mayer, D. Ormanbekova, V. Prade, H. Šimková, T. Wicker, D. Swarbreck, H. Rimbert, M. Felder, N. Guilhot, G. Kaithakottil, J. Keilwagen, P. Leroy, T. Lux, S. Twardziok, L. Venturini, A. Juhász, M. Abrouk, I. Fischer, C. Uauy, P. Borrill, R. H. Ramirez-Gonzalez, D. Arnaud, S. Chalabi, B. Chalhoub, A. Cory, R. Datla, M. W. Davey, J. Jacobs, S. J. Robinson, B. Steuernagel, F. van Ex, B. B. H. Wulff, M. Benhamed, A. Bendahmane, L. Concia, D. Latrasse, J. Bartoš, A. Bellec, H. Berges, J. Doležel, Z. Frenkel, B. Gill, A. Korol, T. Letellier, O.-A. Olsen, K. Singh, M. Valárik, E. van der Vossen, S. Vautrin, S. Weining, T. Fahima, V. Glikson, D. Raats, J. Číhalíková, H. Toegelová, J. Vrána, P. Sourdille, B. Darrier, D. Barabaschi, L. Cattivelli, P. Hernandez, S. Galvez, H. Budak, J. D. G. Jones, K. Witek, G. Yu, I. Small, J. Melonek, R. Zhou, T. Belova, K. Kanyuka, R. King, K. Nilsen, S. Walkowiak, R. Cuthbert, R. Knox, K. Wiebe, D. Xiang, A. Rohde, T. Golds, J. Čížková, B. A. Akpinar, S. Biyiklioglu, L. Gao, A. N'Daiye, M. Kubaláková, J. Šafář, F. Alfama, A.-F. Adam-Blondon, R. Flores, C. Guerche, M. Loaec, H. Quesneville, J. Condie, J. Ens, R. Maclachlan, Y. Tan, A. Alberti, J.-M. Aury, V. Barbe, A. Couloux, C. Cruaud, K. Labadie, S. Mangenot, P. Wincker, G. Kaur, M. Luo, S. Sehgal, P. Chhuneja, O. P. Gupta, S. Jindal, P. Kaur, P. Malik, P. Sharma, B. Yadav, N. K. Singh, J. P. Khurana, C. Chaudhary, P. Khurana, V. Kumar, A. Mahato, S. Mathur, A. Sevanthi, N. Sharma, R. S. Tomar, K. Holušová, O. Plíhal, M. D. Clark, D. Heavens, G. Kettleborough, J. Wright, B. Balcárková, Y. Hu, E. Salina, N. Ravin, K. Skryabin, A. Beletsky, V. Kadnikov, A. Mardanov, M. Nesterov, A. Rakitin, E. Sergeeva, H. Handa, H. Kanamori, S. Katagiri, F. Kobayashi, S. Nasuda, T. Tanaka, J. Wu,

F. Cattonaro, M. Jiumeng, K. Kugler, M. Pfeifer, S. Sandve, X. Xun, B. Zhan, J. Batley, P. E. Bayer, D. Edwards, S. Hayashi, Z. Tulpová, P. Visendi, L. Cui, X. Du, K. Feng, X. Nie, W. Tong, L. Wang, Shifting the limits in wheat research and breeding using a fully annotated reference genome. *Science* **361**, eaar7191 (2018).
30. J. Jia, Y. Xie, J. Cheng, C. Kong, M. Wang, L. Gao, F. Zhao, J. Guo, K. Wang, G. Li, D. Cui, T. Hu, G. Zhao, D. Wang, Z. Ru, Y. Zhang, Homology-mediated inter-chromosomal interactions in hexaploid wheat lead to specific subgenome territories following polyploidization and introgression. *Genome Biol.* **22**, 26 (2021).
31. L. Zhao, J. Chen, Z. Zhang, W. Wu, X. Lin, M. Gao, Y. Yang, P. Zhao, S. Xu, C. Yang, Y. Yao, A. Zhang, D. Liu, D. Wang, J. Xiao, Deciphering the transcriptional regulatory network governing starch and storage protein biosynthesis in wheat for breeding improvement. *Adv Sci (Weinh)* **11**, 2401383 (2024).
32. L. Zhao, Y. Yang, J. Chen, X. Lin, H. Zhang, H. Wang, H. Wang, X. Bie, J. Jiang, X. Feng, X. Fu, X. Zhang, Z. Du, J. Xiao, Dynamic chromatin regulatory programs during embryogenesis of hexaploid wheat. *Genome Biol.* **24**, 7 (2023).
33. M. J. Rowley, V. G. Corces, Organizational principles of 3D genome architecture. *Nat. Rev. Genet.* **19**, 789–800 (2018).
34. E. de Wit, E. P. Nora, New insights into genome folding by loop extrusion from inducible degron technologies. *Nat. Rev. Genet.* **24**, 73–85 (2023).
35. A. R. Barutcu, P. G. Maass, J. P. Lewandowski, C. L. Weiner, J. L. Rinn, A TAD boundary is preserved upon deletion of the CTCF-rich *Firre* locus. *Nat. Commun.* **9**, 1444 (2018).
36. Q. Wu, P. Liu, L. Wang, Many facades of CTCF unified by its coding for three-dimensional genome architecture. *J. Genet. Genomics* **47**, 407–424 (2020).
37. I. F. Davidson, J. M. Peters, Genome folding through loop extrusion by SMC complexes. *Nat. Rev. Mol. Cell Biol.* **22**, 445–464 (2021).
38. M. Zhang, H. Huang, J. Li, Q. Wu, ZNF143 deletion alters enhancer/promoter looping and CTCF/cohesin geometry. *Cell Rep.* **43**, 113663 (2024).
39. C. Liu, Y. J. Cheng, J. W. Wang, D. Weigel, Prominent topologically associated domains differentiate global chromatin packing in rice from Arabidopsis. *Nat. Plants* **3**, 742–748 (2017).
40. E. S. Karaaslan, N. Wang, N. Faiß, Y. Liang, S. A. Montgomery, S. Laubinger, K. W. Berendzen, F. Berger, H. Breuninger, C. Liu, Marchantia TCP transcription factor activity correlates with three-dimensional chromatin structure. *Nat. Plants* **6**, 1250–1261 (2020).
41. Z. Li, M. Wang, K. Lin, Y. Xie, J. Guo, L. Ye, Y. Zhuang, W. Teng, X. Ran, Y. Tong, Y. Xue, W. Zhang, Y. Zhang, The bread wheat epigenomic map reveals distinct chromatin architectural and evolutionary features of functional genetic elements. *Genome Biol.* **20**, 139 (2019).
42. Y. Peng, D. Xiong, L. Zhao, W. Ouyang, S. Wang, J. Sun, Q. Zhang, P. Guan, L. Xie, W. Li, G. Li, J. Yan, X. Li, Chromatin interaction maps reveal genetic regulation for quantitative traits in maize. *Nat. Commun.* **10**, 2632 (2019).
43. C. Wei, L. Gao, R. Xiao, Y. Wang, B. Chen, W. Zou, J. Li, E. Mace, D. Jordan, Y. Tao, Complete telomere-to-telomere assemblies of two sorghum genomes to guide biological discovery. *iMeta* **3**, e193 (2024).
44. L. Deng, Q. Zhou, J. Zhou, Q. Zhang, Z. Jia, G. Zhu, S. Cheng, L. Cheng, C. Yin, C. Yang, J. Shen, J. Nie, J.-K. Zhu, G. Li, L. Zhao, 3D organization of regulatory elements for transcriptional regulation in Arabidopsis. *Genome Biol.* **24**, 181 (2023).
45. H. Nordberg, M. Cantor, S. Dusheyko, S. Hua, A. Poliakov, I. Shabalov, T. Smirnova, I. V. Grigoriev, I. Dubchak, The genome portal of the department of energy joint genome institute: 2014 Updates. *Nucleic Acids Res.* **42**, D26–D31 (2014).
46. Y. Liu, Z. Wang, X. Wu, J. Zhu, H. Luo, D. Tian, C. Li, J. Luo, W. Zhao, H. Hao, H. C. Jing, SorGSD: Updating and expanding the sorghum genome science database with new contents and tools. *Biotechnol. Biofuels* **14**, 165 (2021).
47. M. R. Woodhouse, E. K. Cannon, J. L. Portwood, L. C. Harper, J. M. Gardiner, M. L. Schaeffer, C. M. Andorf, A pan-genomic approach to genome databases using maize as a model system. *BMC Plant Biol.* **21**, 385 (2021).
48. A. Vasudevan, S. Cloutier, Lifting of the 1,000 wheat exome project SNPs from Triticum aestivum cv. Chinese Spring assembly RefSeq v1.0 to RefSeq v2.1. *BMC. Res. Notes* **16**, 220 (2023).
49. C. Hao, C. Jiao, J. Hou, T. Li, H. Liu, Y. Wang, J. Zheng, H. Liu, Z. Bi, F. Xu, J. Zhao, L. Ma, Y. Wang, U. Majeed, X. Liu, R. Appels, M. Maccaferri, R. Tuberosa, H. Lu, X. Zhang, Resequencing of 145 landmark cultivars reveals asymmetric sub-genome selection and strong founder genotype effects on wheat breeding in China. *Mol. Plant* **13**, 1733–1751 (2020).
50. F. He, W. Wang, W. B. Rutter, K. W. Jordan, J. Ren, E. Taagen, N. DeWitt, D. Sehgal, S. Sukumaran, S. Dreisigacker, M. Reynolds, J. Halder, S. K. Sehgal, S. Liu, J. Chen, A. Fritz, J. Cook, G. Brown-Guedira, M. Pumphrey, A. Carter, M. Sorrells, J. Dubcovsky, M. J. Hayden, A. Akhunova, P. L. Morrell, L. Szabo, M. Rouse, E. Akhunov, Genomic variants affecting homoeologous gene expression dosage contribute to agronomic trait variation in allopolyploid wheat. *Nat. Commun.* **13**, 826 (2022).
51. S. Li, S. Yu, Y. Zhang, D. Zhu, F. Li, B. Chen, F. Mei, L. Du, L. Ding, L. Chen, J. Song, Z. Kang, H. Mao, Genome-wide association study revealed TaHXK3-2A as a candidate gene controlling stomatal index in wheat seedlings. *Plant Cell Environ.* **45**, 2306–2323 (2022).
52. A. Li, C. Hao, Z. Wang, S. Geng, M. Jia, F. Wang, X. Han, X. Kong, L. Yin, S. Tao, Z. Deng, R. Liao, G. Sun, K. Wang, X. Ye, C. Jiao, H. Lu, Y. Zhou, D. Liu, X. Fu, X. Zhang, L. Mao, Wheat breeding history reveals synergistic selection of pleiotropic genomic sites for plant architecture and grain yield. *Mol. Plant* **15**, 504–519 (2022).
53. S. Cheng, C. Feng, L. U. Wingen, H. Cheng, A. B. Riche, M. Jiang, M. Leverington-Waite, Z. Huang, S. Collier, S. Orford, X. Wang, R. Awal, G. Barker, T. O'Hara, C. Lister, A. Siluveru, J. Quiroz-Chávez, R. H. Ramírez-González, R. Bryant, S. Berry, U. Bansal, H. S. Bariana, M. J. Bennett, B. Bicego, L. Bilham, J. K. M. Brown, A. Burridge, C. Burt, M. Buurman, M. Castle, L. Chartrain, B. Chen, W. Denbel, A. F. Elkot, P. Fenwick, D. Feuerhelm, J. Foulkes, O. Gaju, A. Gauley, K. Gaurav, A. N. Hafeez, R. Han, R. Horler, J. Hou, M. S. Iqbal, M. Kerton, A. Kondic-Spica, A. Kowalski, J. Lage, X. Li, H. Liu, S. Liu, A. Lovegrove, L. Ma, C. Mumford, S. Parmar, C. Philp, D. Playford, A. M. Przewieslik-Allen, Z. Sarfraz, D. Schafer, P. R. Shewry, Y. Shi, G. A. Slafer, B. Song, B. Song, D. Steele, B. Steuernagel, P. Tailby, S. Tyrrell, A. Waheed, M. N. Wamalwa, X. Wang, Y. Wei, M. Winfield, S. Wu, Y. Wu, B. B. H. Wulff, W. Xian, Y. Xu, Y. Xu, Q. Yuan, X. Zhang, K. J. Edwards, L. Dixon, P. Nicholson, N. Chayut, M. J. Hawkesford, C. Uauy, D. Sanders, S. Huang, S. Griffiths, Harnessing landrace diversity empowers wheat breeding. *Nature* **632**, 823–831 (2024).
54. H. Zhang, Z. Jin, F. Cui, L. Zhao, X. Zhang, J. Chen, J. Zhang, Y. Li, Y. Li, Y. Niu, W. Zhang, C. Gao, X. Fu, Y. Tong, L. Wang, H. Q. Ling, J. Li, J. Xiao, Epigenetic modifications regulate cultivar-specific root development and metabolic adaptation to nitrogen availability in wheat. *Nat. Commun.* **14**, 8238 (2023).
55. J. Qi, Q. Qian, Q. Bu, S. Li, Q. Chen, J. Sun, W. Liang, Y. Zhou, C. Chu, X. Li, F. Ren, K. Palme, B. Zhao, J. Chen, M. Chen, C. Li, Mutation of the rice Narrow leaf1 gene, which encodes a novel protein, affects vein patterning and polar auxin transport. *Plant Physiol.* **147**, 1947–1959 (2008).
56. D. Du, Z. Li, J. Yuan, F. He, X. Li, N. Wang, R. Li, W. Ke, D. Zhang, Z. Chen, Z. Jiang, Y. Liu, L. Chai, J. Liu, Z. Hu, W. Guo, H. Peng, Y. Yao, Q. Sun, Z. Ni, M. Xin, The TaWAK2-TaNAL1-TaDST pathway regulates leaf width via cytokinin signaling in wheat. *Sci. Adv.* **10**, eadp5541 (2024).
57. P. Zhao, Z. Liu, X. Shi, W. Hou, M. Cheng, Y. Liu, J. Simmonds, W. Ji, C. Uauy, S. Xu, X. Wang, Modern wheat breeding selection synergistically improves above- and belowground traits. *Plant Physiol.* **196**, 47–50 (2024).
58. R. H. Ramírez-González, P. Borrill, D. Lang, S. A. Harrington, J. Brinton, L. Venturini, M. Davey, J. Jacobs, F. van Ex, A. Pasha, Y. Khedikar, S. J. Robinson, A. T. Cory, T. Florio, L. Concia, C. Juery, H. Schoonbeek, B. Steuernagel, D. Xiang, C. J. Ridout, B. Chalhoub, K. F. X. Mayer, M. Benhamed, D. Latrasse, A. Bendahmane, International Wheat Genome Sequencing Consortium, B. B. H. Wulff, R. Appels, V. Tiwari, R. Datla, F. Choulet, C. J. Pozniak, N. J. Provart, A. G. Sharpe, E. Paux, M. Spannagl, A. Bräutigam, C. Uauy, A. Korol, A. G. Sharpe, A. Juhász, A. Rohde, A. Bellec, A. Distelfeld, B. A. Akpinar, B. Keller, B. Darrier, B. Gill, B. Chalhoub, B. Steuernagel, C. Feuillet, C. Chaudhary, C. Uauy, C. Pozniak, D. Ormanbekova, D. Xiang, D. Latrasse, D. Swarbreck, D. Barabaschi, D. Raats, E. Sergeeva, E. Salina, E. Paux, F. Cattonaro, F. Choulet, F. Kobayashi, G. Keeble-Gagnere, G. Kaur, G. Muehlbauer, G. Kettleborough, G. Yu, H. Šimková, H. Gundlach, H. Berges, H. Rimbert, H. Budak, H. Handa, I. Small, J. Bartoš, J. Rogers, J. Doležel, J. Keilwagen, J. Poland, J. Melonek, J. Jacobs, J. Wright, J. D. G. Jones, J. Gutierrez-Gonzalez, K. Eversole, K. Nilsen, K. F. X. Mayer, K. Kanyuka, K. Singh, L. Gao, L. Concia, L. Venturini, L. Cattivelli, M. Spannagl, M. Mascher, M. Hayden, M. Abrouk, M. Alaux, M. Luo, M. Valárik, M. Benhamed, N. K. Singh, N. Sharma, N. Guilhot, N. Ravin, N. Stein, O.-A. Olsen, O. P. Gupta, P. Khurana, P. Chhuneja, P. E. Bayer, P. Borrill, P. Leroy, P. Rigault, P. Sourdille, P. Hernandez, R. Flores, R. H. Ramirez-Gonzalez, R. King, R. Knox, R. Appels, R. Zhou, S. Walkowiak, S. Galvez, S. Biyiklioglu, S. Nasuda, S. Sandve, S. Chalabi, S. Weining, S. Sehgal, S. Jindal, T. Belova, T. Letellier, T. Wicker, T. Tanaka, T. Fahima, V. Barbe, V. Tiwari, V. Kumar, Y. Tan, The transcriptional landscape of polyploid wheat. *Science* **361**, eaar6089 (2018).
59. R. Stadhouders, G. J. Filion, T. Graf, Transcription factors and 3D genome conformation in cell-fate decisions. *Nature* **569**, 345–354 (2019).
60. Y. Zhang, Z. Li, J. Liu, Y. Zhang, L. Ye, Y. Peng, H. Wang, H. Diao, Y. Ma, M. Wang, Y. Xie, T. Tang, Y. Zhuang, W. Teng, Y. Tong, W. Zhang, Z. Lang, Y. Xue, Y. Zhang, Transposable elements orchestrate subgenome-convergent and -divergent transcription in common wheat. *Nat. Commun.* **13**, 6940 (2022).
61. Y. Wang, H. Qin, J. Ni, T. Yang, X. Lv, K. Ren, X. Xu, C. Yang, X. Dai, J. Zeng, W. Liu, D. Xu, W. Ma, Genome-wide identification, characterization and expression patterns of the DBB transcription factor family genes in wheat. *Int. J. Mol. Sci.* **25**, 11654 (2024).
62. H. Pei, W. Teng, L.-f. Gao, H. Gao, X. Ren, Y. Liu, J. Jia, Y. Tong, Y. Wang, Z. Lu, Low-affinity SPL binding sites contribute to subgenome expression divergence in allohexaploid wheat. *Sci. China Life Sci.* **66**, 819–834 (2022).
63. W. Zhang, K. Peng, F. Cui, D. Wang, J. Zhao, Y. Zhang, N. Yu, Y. Wang, D. Zeng, Y. Wang, Z. Cheng, K. Zhang, Cytokinin oxidase/dehydrogenase OsCKX11 coordinates source and sink relationship in rice by simultaneous regulation of leaf senescence and grain number. *Plant Biotechnol. J.* **19**, 335–350 (2021).
64. Z. Lu, W. A. Ricci, R. J. Schmitz, X. Zhang, Identification of *cis*-regulatory elements by chromatin structure. *Curr. Opin. Plant Biol.* **42**, 90–94 (2018).

65. D. K. Saini, Y. Chopra, J. Singh, K. S. Sandhu, A. Kumar, S. Bazzer, P. Srivastava, Comprehensive evaluation of mapping complex traits in wheat using genome-wide association studies. *Mol. Breed.* **42**, 1 (2021).
66. J. H. Sahito, H. Zhang, Z. G. N. Gishkori, C. Ma, Z. Wang, D. Ding, X. Zhang, J. Tang, Advancements and prospects of genome-wide association studies (GWAS) in maize. *Int. J. Mol. Sci.* **25**, 1918 (2024).
67. D. Xiang, T. D. Quilichini, Z. Liu, P. Gao, Y. Pan, Q. Li, K. T. Nilsen, P. Venglat, E. Esteban, A. Pasha, Y. Wang, R. Wen, Z. Zhang, Z. Hao, E. Wang, Y. Wei, R. Cuthbert, L. V. Kochian, A. Sharpe, N. Provart, D. Weijers, C. S. Gillmor, C. Pozniak, R. Datla, The transcriptional landscape of polyploid wheats and their diploid ancestors during embryogenesis and grain development. *Plant Cell* **31**, 2888–2911 (2019).
68. Y. Xie, S. Ying, Z. Li, Y. Zhang, J. Zhu, J. Zhang, M. Wang, H. Diao, H. Wang, Y. Zhang, L. Ye, Y. Zhuang, F. Zhao, W. Teng, W. Zhang, Y. Tong, J. Cho, Z. Dong, Y. Xue, Y. Zhang, Transposable element-initiated enhancer-like elements generate the subgenome-biased spike specificity of polyploid wheat. *Nat. Commun.* **14**, 7465 (2023).
69. Q. Song, T. Zhang, D. M. Stelly, Z. J. Chen, Epigenomic and functional analyses reveal roles of epialleles in the loss of photoperiod sensitivity during domestication of allotetraploid cottons. *Genome Biol.* **18**, 99 (2017).
70. W. A. Whyte, D. A. Orlando, D. Hnisz, B. J. Abraham, C. Y. Lin, M. H. Kagey, P. B. Rahl, T. I. Lee, R. A. Young, Master transcription factors and mediator establish super-enhancers at key cell identity genes. *Cell* **153**, 307–319 (2013).
71. D. M. Emms, S. Kelly, OrthoFinder: Solving fundamental biases in whole genome comparisons dramatically improves orthogroup inference accuracy. *Genome Biol.* **16**, 157 (2015).
72. Y. Long, J. F. Wendel, X. Zhang, M. Wang, Evolutionary insights into the organization of chromatin structure and landscape of transcriptional regulation in plants. *Trends Plant Sci.* **29**, 638–649 (2024).
73. Y. Liu, P. Liu, L. Gao, Y. Li, X. Ren, J. Jia, L. Wang, X. Zheng, Y. Tong, H. Pei, Z. Lu, Epigenomic identification of vernalization *cis*-regulatory elements in winter wheat. *Genome Biol.* **25**, 200 (2024).
74. B. J. Reinhart, E. G. Weinstein, M. W. Rhoades, B. Bartel, D. P. Bartel, MicroRNAs in plants. *Genes Dev.* **16**, 1616–1626 (2002).
75. H. Wang, H. Wang, The miR156/SPL module, a regulatory hub and versatile toolbox, gears up crops for enhanced agronomic traits. *Mol. Plant* **8**, 677–688 (2015).
76. S. Wingett, P. Ewels, M. Furlan-Magaril, T. Nagano, S. Schoenfelder, P. Fraser, S. Andrews, HiCUP: Pipeline for mapping and processing Hi-C data. *F1000Res* **4**, 1310 (2015).
77. R. F. McCormick, S. K. Truong, A. Sreedasyam, J. Jenkins, S. Shu, D. Sims, M. Kennedy, M. Amirebrahimi, B. D. Weers, B. McKinley, A. Mattison, D. T. Morishige, J. Grimwood, J. Schmutz, J. E. Mullet, The Sorghum bicolor reference genome: Improved assembly, gene annotations, a transcriptome atlas, and signatures of genome organization. *Plant J.* **93**, 338–354 (2018).
78. M. B. Hufford, A. S. Seetharam, M. R. Woodhouse, K. M. Chougule, S. Ou, J. Liu, W. A. Ricci, T. Guo, A. Olson, Y. Qiu, R. Della Coletta, S. Tittes, A. I. Hudson, A. P. Marand, S. Wei, Z. Lu, B. Wang, M. K. Tello-Ruiz, R. D. Piri, N. Wang, D. w. Kim, Y. Zeng, C. H. O'Connor, X. Li, A. M. Gilbert, E. Baggs, K. V. Krasileva, J. L. Portwood, E. K. S. Cannon, C. M. Andorf, N. Manchanda, S. J. Snodgrass, D. E. Hufnagel, Q. Jiang, S. Pedersen, M. L. Syring, D. A. Kudrna, V. Llaca, K. Fengler, R. J. Schmitz, J. Ross-Ibarra, J. Yu, J. I. Gent, C. N. Hirsch, D. Ware, R. K. Dawe, De novo assembly, annotation, and comparative analysis of 26 diverse maize genomes. *Science* **373**, 655–662 (2021).
79. Y. Kawahara, M. de la Bastide, J. P. Hamilton, H. Kanamori, W. R. McCombie, S. Ouyang, D. C. Schwartz, T. Tanaka, J. Wu, S. Zhou, K. L. Childs, R. M. Davidson, H. Lin, L. Quesada-Ocampo, B. Vaillancourt, H. Sakai, S. S. Lee, J. Kim, H. Numa, T. Itoh, C. R. Buell, T. Matsumoto, Improvement of the Oryza sativa Nipponbare reference genome using next generation sequence and optical map data. *Rice (NY)* **6**, 4 (2013).
80. T. Zhu, L. Wang, H. Rimbert, J. C. Rodriguez, K. R. Deal, R. De Oliveira, F. Choulet, G. Keeble-Gagnère, J. Tibbits, J. Rogers, K. Eversole, R. Appels, Y. Q. Gu, M. Mascher, J. Dvorak, M. C. Luo, Optical maps refine the bread wheat Triticum aestivum cv. Chinese Spring genome assembly. *Plant J* **107**, 303–314 (2021).
81. H. Li, R. Durbin, Fast and accurate long-read alignment with Burrows-Wheeler transform. *Bioinformatics* **26**, 589–595 (2010).
82. N. Servant, N. Varoquaux, B. R. Lajoie, E. Viara, C. J. Chen, J. P. Vert, E. Heard, J. Dekker, E. Barillot, HiC-Pro: An optimized and flexible pipeline for Hi-C data processing. *Genome Biol.* **16**, 259 (2015).
83. J. Feng, T. Liu, B. Qin, Y. Zhang, X. S. Liu, Identifying ChIP-seq enrichment using MACS. *Nat. Protoc.* **7**, 1728–1740 (2012).
84. J. Wolff, L. Rabbani, R. Gilsbach, G. Richard, T. Manke, R. Backofen, B. A. Grüning, Galaxy HiCExplorer 3: A web server for reproducible Hi-C, capture Hi-C and single-cell Hi-C data analysis, quality control and visualization. *Nucleic Acids Res.* **48**, W177–W184 (2020).
85. K. C. Akdemir, L. Chin, HiCPlotter integrates genomic data with interaction matrices. *Genome Biol.* **16**, 198 (2015).
86. A. Kechin, U. Boyarskikh, A. Kel, M. Filipenko, cutPrimers: A new tool for accurate cutting of primers from reads of targeted next generation sequencing. *J. Comput. Biol.* **24**, 1138–1143 (2017).
87. A. M. Bolger, M. Lohse, B. Usadel, Trimmomatic: A flexible trimmer for Illumina sequence data. *Bioinformatics* **30**, 2114–2120 (2014).
88. A. Dobin, C. A. Davis, F. Schlesinger, J. Drenkow, C. Zaleski, S. Jha, P. Batut, M. Chaisson, T. R. Gingeras, STAR: Ultrafast universal RNA-seq aligner. *Bioinformatics* **29**, 15–21 (2013).
89. B. Li, C. N. Dewey, RSEM: Accurate transcript quantification from RNA-Seq data with or without a reference genome. *BMC Bioinformatics* **12**, 323 (2011).
90. M. D. Robinson, D. J. McCarthy, G. K. Smyth, edgeR: A bioconductor package for differential expression analysis of digital gene expression data. *Bioinformatics* **26**, 139–140 (2010).
91. D. V. Klopfenstein, L. Zhang, B. S. Pedersen, F. Ramírez, A. Warwick Vesztrocy, A. Naldi, C. J. Mungall, J. M. Yunes, O. Botvinnik, M. Weigel, W. Dampier, C. Dessimoz, P. Flick, H. Tang, GOATOOLS: A python library for gene ontology analyses. *Sci. Rep.* **8**, 10872 (2018).
92. B. Langmead, S. L. Salzberg, Fast gapped-read alignment with Bowtie 2. *Nat. Methods* **9**, 357–359 (2012).
93. H. Thorvaldsdóttir, J. T. Robinson, J. P. Mesirov, Integrative genomics viewer (IGV): High-performance genomics data visualization and exploration. *Brief. Bioinform.* **14**, 178–192 (2012).
94. A. R. Quinlan, I. M. Hall, BEDTools: A flexible suite of utilities for comparing genomic features. *Bioinformatics* **26**, 841–842 (2010).
95. Y. Chen, W. Song, X. Xie, Z. Wang, P. Guan, H. Peng, Y. Jiao, Z. Ni, Q. Sun, W. Guo, A collinearity-incorporating homology inference strategy for connecting emerging assemblies in the triticeae tribe as a pilot practice in the plant pangenomic era. *Mol. Plant* **13**, 1694–1708 (2020).
96. S. Heinz, C. Benner, N. Spann, E. Bertolino, Y. C. Lin, P. Laslo, J. X. Cheng, C. Murre, H. Singh, C. K. Glass, Simple combinations of lineage-determining transcription factors prime cis-regulatory elements required for macrophage and B cell identities. *Mol. Cell* **38**, 576–589 (2010).
97. T. Wu, E. Hu, S. Xu, M. Chen, P. Guo, Z. Dai, T. Feng, L. Zhou, W. Tang, L. Zhan, X. Fu, S. Liu, X. Bo, G. Yu, clusterProfiler 4.0: A universal enrichment tool for interpreting omics data. *Innovation (Camb)* **2**, 100141 (2021).
98. K. J. Livak, T. D. Schmittgen, Analysis of relative gene expression data using real-time quantitative PCR and the $2^{-\Delta\Delta}C_T$ method. *Methods* **25**, 402–408 (2001).
99. W. Li, F. Zhang, R. Wu, L. Jia, G. Li, Y. Guo, C. Liu, G. Wang, A novel N-methyltransferase in arabidopsis appears to feed a conserved pathway for nicotinate detoxification among land plants and is associated with lignin biosynthesis. *Plant Physiol.* **174**, 1492–1504 (2017).
100. A. Zhou, Y. Bu, T. Takano, X. Zhang, S. Liu, Conserved V-ATPase c subunit plays a role in plant growth by influencing V-ATPase-dependent endosomal trafficking. *Plant Biotechnol. J.* **14**, 271–283 (2016).

Acknowledgments: We thank Y. Tong (Institute of Genetics and Developmental Biology, Chinese Academy of Sciences) for the *Taspl7&15*-CR mutants and C. Zhang (Plant Science Facility of the Institute of Botany, Chinese Academy of Sciences) for the help on the measurement of photosynthetic capacity and Y. Zhou (Peking University) and L. Cui (Jiangxi Agricultural University) for the comments on the manuscript. We thank the China National GenBank (CNGB) for the support they provided. **Funding:** This research was supported by the National Science and Technology Major Project (2023ZD04073), the National Key Research and Development Program of China (2021YFD1201500), the Beijing Natural Science Foundation Outstanding Youth Project (JQ23026), and the CAS Project for Young Scientists in Basic Research (YSBR-093). **Author contributions:** Conceptualization: J.X., Z.Z., X. Lin, and X. Liu. Methodology: J.K. and F.L. Validation: J.K., X. Lin, Y.S., W.W., J.X. and X. Luo. Formal analysis: Z.Z., P.Z., Y.L. and X. Luo. Investigation: J.K., X. Lin, Y.S., W.W., Y.Y., X. Li, P.Z. and X. Luo. Resources: J.K., X. Lin, X. Liu, Y.Y., and X. Luo. Data curation: Z.Z. Writing—original draft: J.X., Z.Z., J.K., X. Lin, and X. Luo. Writing—review and editing: J.X., Z.Z., J.K., X. Lin, C.L., F.L. and S.X. Visualization: J.X., Z.Z., X. Lin, P.Z. and F.L. Supervision: J.X. and X. Liu. Project administration: J.X., X. Lin and X. Liu. Funding acquisition: J.X., X. Lin, and X. Liu. **Competing interests:** The authors declare that they have no competing interests. **Data and materials availability:** Sequencing data of TAC-C, ATAC-seq, and RNA-seq are available at both Genome Sequence Archive of the National Genomics Data Center, China National Center (PRJCA036992) and the China National GeneBank Database (CNP0006876). The code used for all processing and analysis is available in both GitHub (https://github.com/ZhangZhaoheng24/TAC-C) and Zenodo (https://zenodo.org/records/14991699). OCEAN-C, ATAC-seq, Hi-C, ChIP-seq, and DAP-seq data using this study were generated by previous studies (*25, 28, 41, 60, 62, 68*). All other data needed to evaluate the conclusions in this paper are present in the paper and the Supplementary Materials.

Submitted 15 November 2024
Accepted 24 April 2025
Published 30 May 2025
10.1126/sciadv.adu6565